Escola Tècnica Superior d'Enginyers
de Camins, Canals i Ports de Barcelona
UNIVERSITAT POLITÈCNICA DE CATALUNYA

MASTER THESIS

Master

Civil Engineering

Title

Numerical simulation of the dynamics of fluid membranes

Author

Laurence Grosjean

Tutor

Marino Arroyo

Speciality

Computational Mechanics

Date

July 2008

Universitat Politècnica de Catalunya
Programa de Master d'Enginyeria Civil

Departament de Matemàtica Aplicada III

Numerical simulation of the dynamics of fluid membranes

by Laurence Grosjean

Final Project
Advisor: Marino Arroyo

Barcelona, June 2008

Abstract

Numerical simulation of the dynamics of fluid membranes

Laurence Grosjean

The goal of this project is to explore the mechanics of lipid fluid membranes as found in biological and made-man systems through continuum models and numerical simulations. Traditionally, the focus has been on the equilibrium configurations of vesicles through minimization of the curvature energy subject to constraints. Here, the goal is to describe the time-evolution of out-of-equilibrium vesicle configurations, which are of relevance in biological systems. Towards this goal, an accurate description of the dissipative mechanisms is crucial, in particular the viscous dissipation induced by the 2D flow of lipids on the deforming surface that describes a vesicle [1]. The resulting equations can only be solved analytically in very simple settings. So the problem is solved numerically using a B-Spline description of the membrane vesicle. The dynamics are described using two types of viscosity: the $L2$ or Willmore viscosity and the inner flow viscosity. By comparing the evolution in time of the two systems, it is stated that the dynamics are clearly different. It is found that one describes better the physics of the system.

Acknowledgments

I would like to thank my Master thesis supervisor, Prof. Marino Arroyo. With his enthusiasm, his patience and his great efforts to explain things clearly and simply, he helped to make this subject very interesting for me. I also want to express my gratitude for the confidence he gave to me all during my work and for the opportunity of working on this intersting subject. Throughout my final-project-writing period, he provided encouragement, sound advice, good teaching and lots of good ideas.

I would like to thank my profesors in Belgium who gave me the opportunity to go studying one year abroad at the Universitat Politécnica de Catalunya and to develop my final project there, particularly Dr. Laurent Stainier et Prof. Jean-Philippe Ponthot. They gave me advice all during this year and provided encouragement.

I want to express my gratitude to all the personal of LaCaN who was always there to help me, give me intersting advice and share their exprerience. For their kind assistance with giving wise advice, helping with various applications, I wish to thank in addition Régis Cottereau and Adrian Rosolen.

I am indebted to my many student colleagues for providing a stimulating environment in which to learn. I wish to thank all the friends at university (both in Liège and Barcelone), for helping me getting through the difficult times, and for all the emotional support, and caring they provided until the end of my project.

I wish to thank the jury for the attention they will give to my work.

I would like to thank my family for all the support they gave to me during these five years of study. Especially my brothers, my parents and my grand-parents who raised me, supported me, and loved me.

I wish to thank Béatrice Palau and Eric Grosjean for their re-reading and their time.

Contents

List of Figures

List of Tables

Chapter 1

Introduction

1.1 Motivation

The ability to separate oneself from the hostile environment and to exchange components with the surroundings made life possible.
The biologic cells (Fig.1.1), as well as the organelles are separated from the exterior by a membrane. They are closed bags which allow the coexistence of different ionic medium. They are impermeable for macromolecules and so, define different compartiments of different compositions. The biomembranes can be seen as a lipid bilayer decorated by amphiphilic proteins (Fig.1.2).

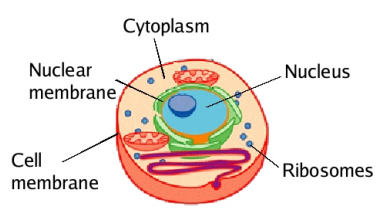

Figure 1.1: Diagram of a cell [2].

The modelling of vesicle is important because we hope to learn the tricks of nature and exploit those for biotechnological applications. Two examples of those appilcation are the use of vesicles for drug delivery systems or the combination of membranes with electronic or optoelectronic devices in order to build biosensors.

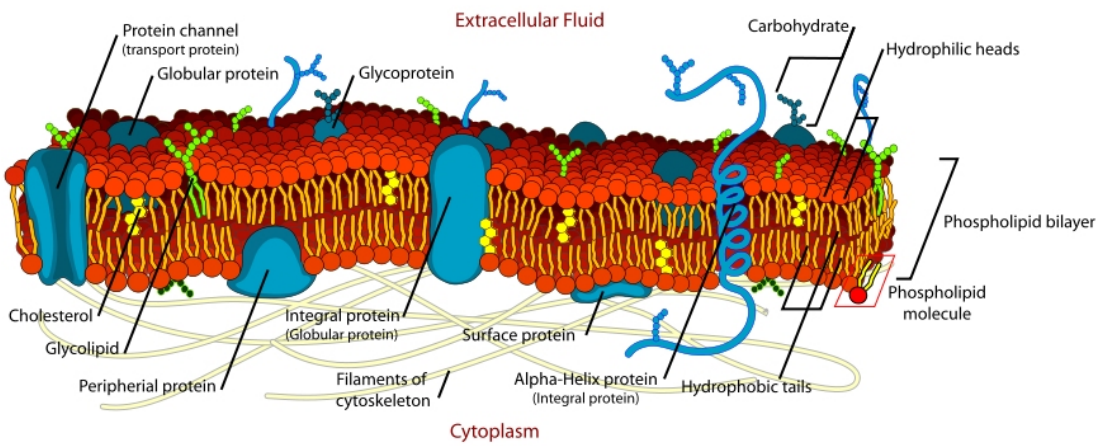

Figure 1.2: Diagram of the biomembrane [3].

Dynamic shape transformations define cells locomotion. Some aspect of these morphological transformations can be studied with closed bag of lipid bilayer in aqueous solutions. This is the simplest system to represent a biological membrane, however it provides interesting results.

Figure 1.3: Discocyte [4].

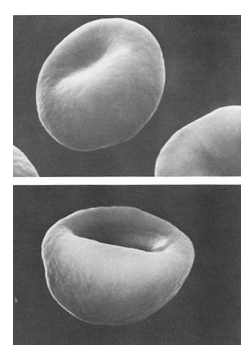

Figure 1.4: Formation of a stomatocyte [5].

The membrane bending energy stabilizes the cell shapes or drives on the shape transitions. The study of the dynamics gives us a large variety of shapes that one can organise in a phase diagram depending on the parameters (spontaneous curvature

and reduced volume in this case).
There are two branches of different shapes: the oblate-branch and the prolate-branch. The first one displays, for example, the change of shape of a red blood cell with the concentration of cholesterol (Fig.1.3 and Fig.1.4). The last one is related to the budding of the cells (Fig.1.5).

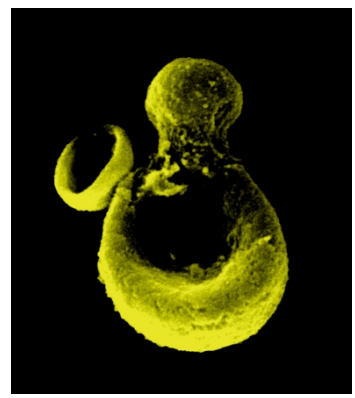

Figure 1.5: Pear-shaped - budding [6].

1.2 Outline

To model the dynamics of vesicles, we proceed as follows.
In the first chapter, some biological explanations are given. The objectives are explained and the mathematical model is developed under some hypothesis.
The second chapter deals with the implementation of the model. The finite elements model is elaborated. The B-Splines are briefly expounded. The curve and its parameters are worked out. Then, the numerical integration is explained.
In the third chapter, the static study of the vesicle is made. The different equilibriums are worked out and paths in the phase diagram are followed.
The fourth chapter talks about the dynamic study. Two different viscosities are implemented and compared.

Chapter 2

Mathematical model

2.1 Biophysics of vesicles

2.1.1 Bending elasticity and spontaneous curvature model

In equilibrium, we can neglect some processes like the hydrodynamic flows or the transport related to temperature gradients. Then, the vesicles will take the shape which minimizes their total energy. To model it, we take into account some features of lipid bilayers (Fig.2.1).

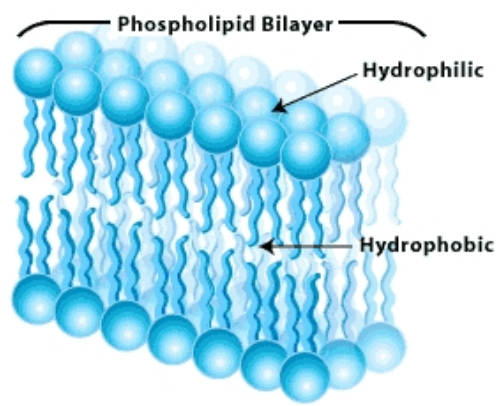

Figure 2.1: Diagram of the lipid bilayer [7].

First, the thickness of the bilayer is in the nanometer range while the size of the vesicles is two or three orders larger. This observation will allow us to describe the vesicle membrane like a closed two-dimensional surface embedded in three-dimensional space. Second, we suppose that the lipid bilayer is in a fluid state, so it does not resist shear forces in the lateral plane. Third, the membrane is supposed to be insoluble, that means that the number of molecules in it is constant. Finally, the two monolayers are allowed to glide over each other and sometimes to exchange molecules[1].

The 2D surface which represents the lipid bilayers can be locally characterized by the two radii of curvature R_1 and R_2 which carry a sign (Fig.2.2).

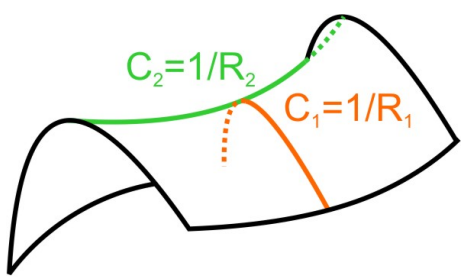

Figure 2.2: Principal curvatures of a surface.

The mean and the Gaussian curvature are respectively defined as

$$H = \left(\frac{1}{R_1} + \frac{1}{R_2}\right) \qquad K = \frac{1}{R_1 R_2}.$$

The spontaneous curvature model for vesicles is based on the assumption that we can define a local energy density f_1 associated to the mean and the Gaussian curvature

$$f_1 = \frac{\kappa}{2}(H - C_0)^2 + \kappa_G K$$

where there are three material parameters: κ, κ_G and C_0.

[1]This is characterized by the spontaneous curvature C_0.

The bending rigidity κ, can be evaluated whereas the Gaussian bending rigidity κ_G is difficult to measure. The spontaneous curvature C_0 is used to represent an asymmetry of the membrane. For instance, the number of lipids can be greater or/and the "head" of the lipids can be larger in one monolayer than in the other. Moreover, the chemical environment on both sides can be different. This parameter is supposed to be laterally homogeneous, it does not depend on the local shape of the membrane.

We can take a term of density of lipids into account but it is known that it is not coupled to the shape and that the energy is minimum for a uniform density [8].

On the other hand, the changes of area are negligeable because of the insolubility of the lipid bilayers. The volume can either be taken as constant or not, it depends on the osmostic pressure. The cells contain water and additional molecules (ions or impureties) which can pass the membrane thanks to different pumps. If there is change of the ionic concentration of the vesicle or of the surroundings, the water will pass the membrane to equilibrate the osmotic pressure and so the volume will change. The figure 2.3 explains this fact: the ions are represented in red. As the concentration of ions is greater in the cell than in the aqueous solution, water goes into the cell to equilibrate the osmotic pressure and so, the volume increases.

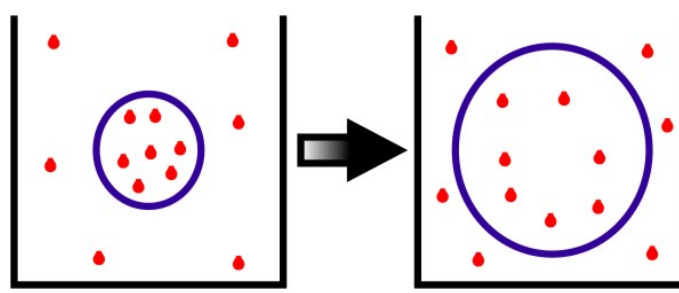

Figure 2.3: Effects of the osmotic pressure.

The total energy is obtained by integration of the local energy over the surface of

the closed vesicle. Noting that the integral of the Gaussian curvature over a closed surface is a topological invariant, and that we will not consider topological changes, this term can be ignored [8] and we are left with the expression for the curvature energy

$$E_{HC} = \int \frac{\kappa}{2} (H - C_0)^2 \, dS \tag{2.1}$$

This expression has to be minimized at constant total enclosed volume and constant surface S to find the equilibrium shape.

2.1.2 Material parameters

Bending rigidity

Great effort has been devoted in order to determine the bending rigidity κ. Three different methods can be distinguished: mechanical, mechanical and entropic and thermally excited membrane fluctuations approach.

For the same lipid, the value of κ obtained by the different methods can differ of a factor two. Furthermore, the same method applied by different research groups yields different values (further analysis is needed to know if theses differences are due to impurities or experimental effects).

Here are some experimental values of the bending rigidity κ for different lipids [8]:

Lipid	$\kappa\,[10^{-19}J]$	Method
DMPC	1.15 ± 0.15	Flickering of quasi-spherical vesicles
DMPC	0.56 ± 0.06	Entropic tension, micropipet
DGDG	$0.12 - 0.27$	Fluctuations of planar pieces
DGDG	0.44 ± 0.3	Entropic tension, micropipet
EYPC	1.15 ± 0.15	Flickering of quasi-spherical vesicles
EYPC	0.8	Fluctuations of planar pieces

Table 2.1: Value of bending rigidity for different lipids and methods.

2.2 Equations and hypothesis

2.2.1 Mechanisms of the problem

For fluid membranes, the inertial forces are negligible. So, the flow is a Stokes flow and acts as a dissipative force opposed to the rate of change of the driving forces (forces induced by the curvature for example).
The dynamics of the fluid membrane are the result of the balance between the driving forces and the dissipation forces, under some constraints.

The energetic driving forces only depend on the configuration of the vesicle.
The first one is the curvature elasticity (eq.2.1) which can promote a spontaneous curvature different from zero. This parameter can change with the flip-flop diffusion of the lipids at very long time scales.
The second one is the line tension that exists in multi-components vesicles. It promotes the budding of vesicles.

Two dissipative mechanisms depend on the rate of change of the system.
First, we can consider the dissipation caused by the reorganization of the bilayers'

particles with the change of configuration. We call it the inner viscosity.
Second, the outer viscosity is the dissipation due to the disturbances caused to the surrounding fluid by the change of configuration.

The constraints reckoned are the inextensibility of the membrane and sometimes the incompressibility of the surrounding fluid. The forces acting on the membrane are generally small, so the lipid bilayer can be considered as inextensible and we need to preserve locally the area. Moreover, as seen before, the volume of the vesicle is function of the osmotic pressure. It will be constant in the static study and constant or not in the dynamic part depending on the case studied.

This list of mechanisms is not exhaustive, for example some research has been done about interlayer slip and friction, swelling and osmotic pressure effects or energetic forces due to membrane-bound actin networks.

2.2.2 Hypothesis

In this work, we implement a particular case of vesicle: the axisymmetric case. Moreover, we only study the vesicle of one component, then we do not have to evaluate the tension line as an energetic driving force. Finally, we neglect the outer flow dissipation, which is a correct assumption for small vesicle or very viscous membrane[2] [1].

2.2.3 Parametrization invariance

The physics of the model is invariant with respect to re-parametrizations. This means that the choice of the parameters does not change the values of the energies, volume and area of the problem.

[2]The very viscous membrane can be a membrane of polymerosomes.

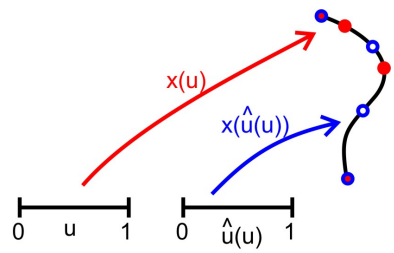

Figure 2.4: Invariance of the parametrization.

Considering the initial parametrization

$$\mathbf{x}(u) : [0,1] \longmapsto \mathbb{R}^2$$

and the strictly increasing change of variables

$$\hat{u} : [0,1] \longmapsto [0,1]$$

then, one can write

$$E_{HC}\left[\mathbf{x}(u)\right] = E_{HC}\left[\mathbf{x}(\hat{u}\,(u))\right]$$

likewise for the other energies, rates of change of energy, volume and area calculated.

2.2.4 Equations

The first reference dealing with fluid dynamics in the interfacial state is Sriven [9] who studies the mechanics of insoluble surface films and foam stability. These equations make extensive use of the covariant derivative, and therefore the pratical calculations are complex. The latter contributions of research did not lead to easier equations. Recently, M.Arroyo and A. DeSimone derived equations governing the flow of two dimensional fluid moving on a surface in the Euclidean space evolving in time which

are easier to compute numerically and analytically [1].

In the static part of the project, we only use the curvature energy E_{HC} (eq.2.1). The minimization of this energy is made under different constraints to find the equilibrium shape. The two first restrictions are the invariance of the area and of the volume. One more restriction due to the parametrization will be added later.

The dynamic of the axisymmetric problem is described using two different viscous dissipations.
First, we consider L_2 dissipation related to the Willmore flow defined as

$$W_{L_2}[v_n] = \frac{\hat{\mu}}{2} \int_\Gamma v_n^2 dS \tag{2.2}$$

and second, the physical inner flow dissipation [1]

$$W_D[v_t, v_n] = \mu \int_\Gamma \left\{ \left(\frac{1}{a} v_t' \right)^2 + \left(\frac{r'}{ar} v_t \right)^2 - \frac{2v_n}{a} \left(\frac{b}{a^3} v_t' + \frac{z'r'}{ar^2} v_t \right) + (H^2 - 2K) v_n^2 \right\} dS \tag{2.3}$$

where $v_t = av$ (a is defined later (eq.3.1))[3].

We will consider two dynamic cases:

- The explicit scheme for the L_2 dissipation
- The explicit scheme for the physical inner flow dissipation

The constraints taken for these different cases are explained in the dynamic part of this study.

[3]It is necessary to multiply v by a because $\frac{\partial}{\partial u}$ is not a unit vector.

Chapter 3

Implementation

3.1 Introduction

The representation of the curve is made using B-Splines. We first parametrize the surface in the r-z plane and calculate its different geometric parameters (mean curvature, gaussian curvature) which do not change with the parametrization (section 2.2.3). The numerical integration of Gauss-Legendre is used to evaluate the global parameters of the curve (volume, area, energy) and the boundary conditions are enforced.

3.2 Finite element discretization

As we study an axisymmetric case, all the parameters are independent of the angle θ and we only need a curve in the $r - z$ plane to describe the 2D surface of the vesicle (Fig.3.1).

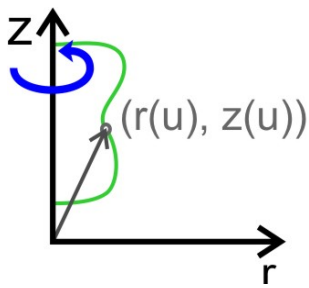

Figure 3.1: Plane of the parametrization.

If the coordinates of every points of the $2D$ curve in the r-z plane are known, the coordinates in the $3D$ space can be found with

$$\begin{aligned} y_{3D} &= r_{2D}\, sin\theta \\ r_{3D} &= r_{2D}\, cos\theta \\ z_{3D} &= z_{2D} \end{aligned}$$

with $\theta \in [0, 2\pi]$.

3.2.1 B-Splines

The two most used methods to represent a curve in space are the implicit equations and the parametric functions.
The implicit equations are implicit relations between the coordinates r and z of the point on the curve ($f(r, z) = 0$) whereas the parametric functions represent each of the coordinates of the point on the curve as an explicit function of an independent parameter u ($x(u) = \cos(u)$, $y(u) = \sin(u)$, $a \leqslant u \leqslant b$). Therefore, the parametrization is not unique.

The parametric description of a curve has some advantages. The description is more natural in computer code and the algorithms are numerically stable. However, sometimes, one has to deal with parametric anomalies (like the poles in a circle which are the same points as the others geometrically but have difficulties of calculations in

parametric representation).

In this study, the choice made is to use a parametric description of the curve: the B-Splines. The curve is defined by

$$\mathbf{C}(u) = \sum_{i=1}^{N+1} N_i(u)\mathbf{P_i}$$

where $N_i(u)$ is the ith basis function and $\mathbf{P_i}$ is the vector of coordinates (r, z) of the ith control point. The control points define the control polygon which supports the curve drawed (Fig.3.2).

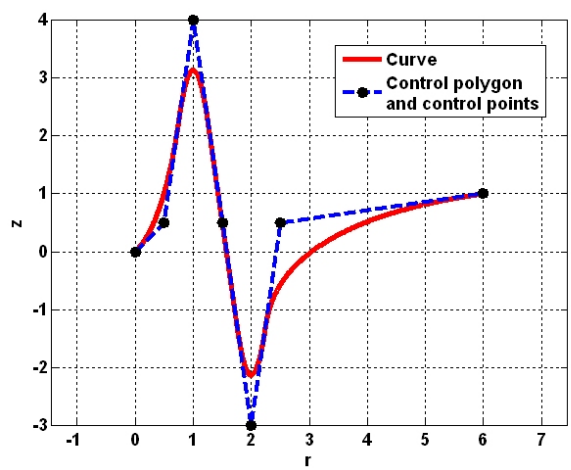

Figure 3.2: Control polygon.

The basis function used are B-Splines of second order ($p = 2$) because we need C^1 continuity[1]. They are piecewise polynomial with some useful properties like convex hull, variation diminishing, transformation invariance and local support [10]. The last propriety is very interesting: the change of the position of one control point only has consequences in the neighbourhood of this point (Fig.3.3).

[1]The second derivatives are necessary, so the C^1 is the less restrictive condition to have a second order derivative defined.

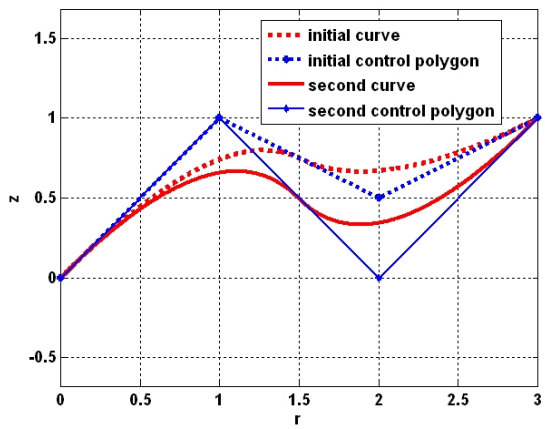

Figure 3.3: B-Splines - propriety of local support.

The definition of the basis functions changes at the breakpoints. In figure 3.4, each dot line represents a breakpoint and every different second order polynome is drawn in another color.

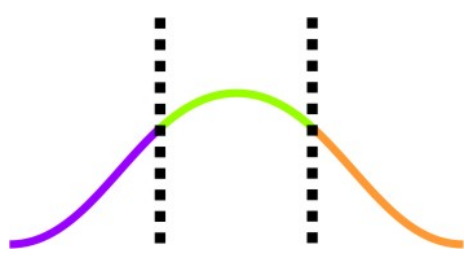

Figure 3.4: Definition of a second order basis function.

The knot vector (vector of breakpoints[2]) $\mathbf{U}$, is taken non-periodic and uniform[3]. That means that its form is

[2]Or vector of knot, no difference is made here.

[3]The order of continuity is equal to $p - k$, as $p = 2$ and as C^1 continuity is needed, $k = 1$, with k the multiplicity of the knot.

$$U = \left\{ \overbrace{\underbrace{0,0,0}_{p+1=3}, u_{p+1}, \cdots, u_{m-p-1}, \underbrace{1,1,1}_{p+1=3}}^{m+1} \right\}$$

where the number of knots in the knot vector is $m+1$, the number of control points is $N+1$ and the link between m and N for a non-periodic and uniform knot vector is $N = m - p - 1$.
As the order of the shape functions is fixed ($p = 2$), one can remark that the length of the knot vector is totally defined by the numbers of control points ($N+1$).

The ith B-Spline basis function of p-degree, denoted by $N_{i,p}(u)$ is defined as [10]:

$$N_{i,0}(u) = \begin{cases} 1 & \text{if } u_i \leqslant u < u_{i+1} \\ 2 & \text{otherwise} \end{cases}$$

$$N_{i,p}(u) = \frac{u - u_i}{u_{i+p} - u_i} N_{i,p-1}(u) + \frac{u_{i+p+1} - u}{u_{i+p+1} - u_{i+1}} N_{i+1,p-1}(u)$$

The illustration of second order basis function for the knot vector

$$U = \left\{ 0,0,0, \frac{1}{6}, \frac{2}{6}, \frac{3}{6}, \frac{4}{6}, \frac{5}{6}, 1,1,1 \right\}$$

is showed at figure 3.5, where the black lines represent the breakpoints.

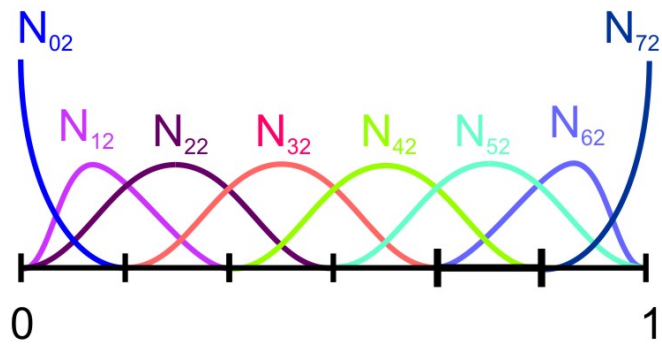

Figure 3.5: Second order B-Splines.

Using the B-Spline representation , it is easy to compute the derivatives of $\mathbf{C}(u)$. Let $\mathbf{C}^{(k)}(u)$ be the kth derivative of $\mathbf{C}(u)$. If u is fixed, we can obtain the derivative by computing the kth derivatives of the basis functions. In particular,

$$\mathbf{C}^{(k)}(u) = \sum_{i=1}^{N+1} N_{i,p}^{(k)} \mathbf{P}_i$$

As we only need the first and the second derivatives of the basis functions, we can apply these two formules [10]:

$$N_{i,p}^{(1)}(u) = 2\left(a_{1,0} N_{i,p-1}(u) + a_{1,1} N_{i+1,p-1}(u)\right)$$

$$N_{i,p}^{(2)}(u) = 2\sum_{j=0}^{2} a_{2,j} N_{i+j,p-2}(u)$$

with

$$\begin{cases} a_{0,0} &= 1 \\ a_{k,0} &= \frac{a_{k-1,0}}{u_{i+p-k+1} - u_i} \\ a_{k,j} &= \frac{a_{k-1,j} - a_{k-1,j-1}}{u_{i+p+j-k+1} - u_{i+j}} \qquad j = 1, ..., k-1 \\ a_{k,k} &= \frac{-a_{k-1,k-1}}{u_{i+p+1} - u_{i+k}} \end{cases}$$

3.2.2 Program used

To implement the code, we use the powerfull mathematic program Matlab which allows us to easily make graphs, programs, movies and optimization because it contains a lot of prepared functions.

We have implemented a lot of files.m in Matlab to describe the curve using B-Splines. The main steps are the following: for a $u \in [0, 1]$ given, the number of the interval related is found, then the values of the basis different from zero are calculated at u. The algorithm implemented is based of the one of [10]. The first and the second derivatives are calculated too. Knowing all of this, the position of the points of the curve and the values of their derivatives can be calculated by assembling.
After, the geometric parameters are easily worked on and the global variables which are necessary to compute with integration are found with Gauss numerical integration.

3.3 Description of the curve

3.3.1 Mathematical process

At first, the supposition is made that the control points are given and the curve related is computed, as well as its geometric parameters.

Each point of the curve is defined with the couple of coordinates (r, z). Knowing the basis functions at a point u of the knot vector, we can find the coordinates of the point on the curve associated

$$\mathbf{C}(u) = \sum_{i=1}^{N+1} N_i(u)\mathbf{P_i} \qquad \text{with} \quad \mathbf{P_i} = \left\{ \begin{array}{c} r_i \\ z_i \end{array} \right\}$$

$$\Rightarrow r(u) = \sum_{i=1}^{N+1} N_i(u) r_i \qquad\qquad z(u) = \sum_{i=1}^{N+1} N_i(u) z_i$$

Recall that $u \in [0,1]$[4].

The derivatives of the curve at the breakpoints can be calculated using the same method

$$r(u)^{(k)} = \sum_{i=1}^{N+1} N_i^{(k)}(u) r_i \qquad\qquad z(u)^{(k)} = \sum_{i=1}^{N+1} N_i^{(k)}(u) z_i$$

Then, the geometric parameters of the curve can be found. The formulation of the mean curvature H in the axisymmetric case is [1]

$$H(u) = \frac{1}{a(u)} \left(\frac{b(u)}{a(u)^2} + \frac{z'(u)}{r(u)} \right) \qquad \text{with} \begin{cases} a^2(u) = (r'(u))^2 + (z'(u))^2 \\ b(u) = -r''(u)z'(u) + r'(u)z''(u) \end{cases} \tag{3.1}$$

and the Gaussian curvature is

$$K(u) = \frac{b(u)z'(u)}{(a(u))^4 r(u)}.$$

After, some global characteristics of the curve like the volume, the area, the curvature energy are needed.
To compute them, it is necessary to evaluate integrals.
As the points are not fixed, the method used is the numerical Gauss integration because it maximizes the order of the quadrature for a number of integration points given[5].

[4]To have a good representation of the curve, it is required to take a very large interpolation vector (1000 components for example).

[5]The basis functions are of order 2, so we need 2 Gauss points by interval to integrate exactly.

Let's take a general case and suppose it is necessary to integrate the function $f(u)$, independent of θ, over the surface. Hence, one can write

$$\int_S f(u)dS = 2\pi \int_{u=0}^{u=1} f(u)a(u)r(u)du \tag{3.2}$$

Moreover, the basis functions are quadratic and they change of definition at every breakpoint. So this integral is divided in a sum of smaller integrals (Fig.3.6). Those are evaluated in an interval contained between two adjacent breakpoints (where the basis functions have the same polynamial definition).

$$2\pi \int_{u=0}^{u=1} f(u)a(u)r(u)du = 2\pi \sum_{i=1}^{m-2p} \int_{u=u_i}^{u=u_{i+1}} f(u)a(u)r(u)du \tag{3.3}$$

The vector of the u_i is of the type $U = \{0, 0.25, 0.5, 0.75, 1\}$[6] and $m - 2p$ is the number of intervals.

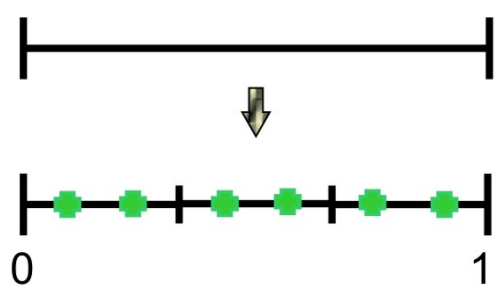

Figure 3.6: Splitting of the interval $[0, 1]$ for the numerical integration. The Gauss points are in green.

Now, to integrate exactly over one interval, the Gauss-Legendre integration with change of variables and two Gauss points[7] is applied and leads to

[6]The same as the knot vector but without repetition of knots.
[7]The case of three and four Gauss points has been implemented too.

$$2\pi \sum_{i=1}^{m-2p} \int_{u=u_i}^{u=u_{i+1}} f(u)a(u)r(u)du = 2\pi \sum_{i=1}^{m-2p} \left(\frac{u_{i+1}-u_i}{2} \sum_{j=1}^{N_g} w_j f(u_{g_{ij}})a(u_{g_{ij}})r(u_{g_{ij}}) \right) \tag{3.4}$$

where $u_{g_{ij}}$ is the jth Gauss point of the ith interval considered and N_g the number of Gauss points considered in each subintervals.

This method can be applied to calculate integrals of a function independent of θ over the area.

To integrate the volume[8], the formule is

$$\begin{aligned} \int_V f(u)dV &= \int_{\theta=0}^{\theta=2\pi} \int_z \int_{r=0}^{r=r(u)} r(u)d\theta \frac{dz}{du} dr du \\ &= -2\pi \int_{u=0}^{u=1} \int_{r=0}^{r=r(u)} r(u)z'(u)dr du \\ &= -2\pi \int_{u=0}^{u=1} \frac{(r(u))^2 z'(u)}{2} du \end{aligned}$$

and then the same method as before can be used to integrate this expression numerically.

3.3.2 Boundary conditions

For the modelization of axisymmetric shapes, it is required to enforce boundary conditions.
We can consider two types of boundary condition depending on the problem resolved.

[8]The sign minus comes from this equality $\frac{dz}{du} = -z'$ which depends on the parametrization chosen.

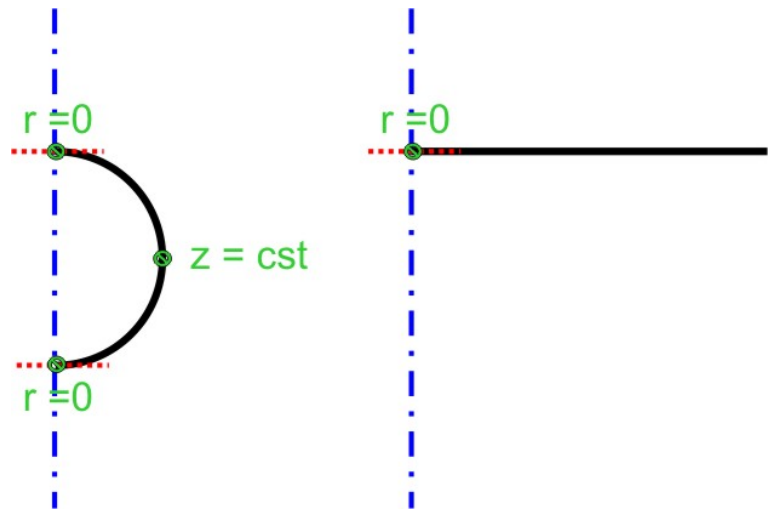

Figure 3.7: Boundary conditions for the closed vesicle (on the left) and the open vesicle (on the right).

Closed vesicle

As the curve computed will be rotated of 2π around the z-axis, the first and the last tangent have to be horizontal (perpendicular to the z-axis). This condition is very easy to set with the B-Splines: the z-coordinates of the two first control points have to be equal. Likewise, the z-coordinates of the two last control points have to be the same.
Moreover, the first and the last points must be on the z-axis. So, the r-coordinates of the first and the last control points have to be zero.
At the end, to prevent the rigid body motions, the z-coordinate of one breakpoint is fixed during all the process. To keep the symmetry, this condition is enforced at the middle-control point (Fig.3.7).

$$z_1 = z_2 \qquad z_{N+1} = z_N$$
$$r_1 = 0 \qquad r_{N+1} = 0$$
$$z_{\text{middle control point}} = \text{constant}$$

Open vesicle

This case is identical to the previous case but without the requirements in the last and the middle point:

$$z_1 = z_2$$
$$r_1 = 0$$

Chapter 4

Static study

4.1 Introduction

In this part, shapes of minimum energy of the membranes are found under constraints of constant enclosed volume and constant area.
Therefore, the curvature energy and its gradient in relation with the control points are calculated in order to find the shape of equilibrium of the vesicle through a matlab optimization function under some boundary conditions.
After, different shapes are found changing the value of the volume and of the spontaneous curvature but keeping the area fixed. Paths in the phase diagram of spontaneous curvature model are done too.

4.2 Research of equilibrium

4.2.1 Mathematical process

The shape of mimimum energy of the vesicle under some constraints is determined using the penalty method which replaces a constrained optimization problem by a series of unconstrained problems whose solutions must converge to the solution of the original constrained problem.

In this study, the constraints are the imposition of a certain volume and a certain area. The problem of minimization of the energy can be written as

$$\min_{\mathbf{P}} F(\mathbf{P}) = E_{HC}(\mathbf{P}) + k_1(V(\mathbf{P}) - V_0) + k_2(S(\mathbf{P}) - S_0) + k_3 A(\mathbf{P})$$

where k_1 , k_2 and k_3 are the constants of penalization, V_0 and S_0 the volume and the area prescribed, $V(\mathbf{P})$ and $S(\mathbf{P})$ the current volume and area and A is an additional constraint due to the parametrization

$$A = \int_S (a'(u))^2 dS = 2\pi \int_{u=0}^{u=1} (a'(u))^2 a(u) r(u) du.$$

In fact $a(u)$ is the velocity or stretching of of the interval $[0, 1]$ into the curve and, with the last restriction, it is imposed to be constant. It prevents the accumulation of all the control points in one part of the curve (Fig.4.1).

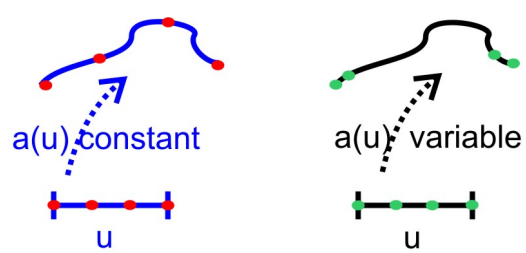

Figure 4.1: Effect of $a(u)$ constant.

The Matlab function FMINCON[1] is used to perform this optimization. Before using this function, one must calculate the gradient of F for each control point.

$$\nabla F = \left(\frac{\partial F}{\partial r}, \frac{\partial F}{\partial z} \right)$$

[1]This function uses a large-scale method to find the equilibrium.

with

$$\frac{\partial F}{\partial r} = \frac{\partial E_{HC}}{\partial r} + 2k_1(V(\mathbf{P}) - V_0)\frac{\partial V(\mathbf{P})}{\partial r} + 2k_2(S(\mathbf{P}) - S_0)\frac{\partial S(\mathbf{P})}{\partial r} + k_3\frac{\partial A(\mathbf{P})}{\partial r}$$

$$\frac{\partial F}{\partial z} = \frac{\partial E_{HC}}{\partial z} + 2k_1(V(\mathbf{P}) - V_0)\frac{\partial V(\mathbf{P})}{\partial z} + 2k_2(S(\mathbf{P}) - S_0)\frac{\partial S(\mathbf{P})}{\partial z} + k_3\frac{\partial A(\mathbf{P})}{\partial z}.$$

Therefore, the computation of the derivatives of $r(u)$, $z(u)$, $a(u)$, $b(u)$, $H(u)$, $a'(u)$ is worked out.

$$\begin{array}{ll}
\frac{\partial r(u)}{\partial r_i} = N_i(u) & \frac{\partial r(u)}{\partial z_i} = 0 \\
\frac{\partial z(u)}{\partial r_i} = 0 & \frac{\partial z(u)}{\partial z_i} = N_i(u) \\
\frac{\partial a(u)}{\partial r_i} = \frac{r'(u)}{a(u)}N_i'(u) & \frac{\partial a(u)}{\partial z_i} = \frac{z'(u)}{a(u)}N_i'(u) \\
\frac{\partial b(u)}{\partial r_i} = -z'(u)N_i''(u) + z''(u)N_i'(u) & \frac{\partial b(u)}{\partial z_i} = -r''(u)N_i'(u) + r'(u)N_i''(u) \\
\frac{\partial (H(u))^2}{\partial r_i} = 2H(u)\frac{\partial H(u)}{\partial r_i} & \frac{\partial (H(u))^2}{\partial z_i} = 2H(u)\frac{\partial H(u)}{\partial z_i}
\end{array}$$

$$\frac{\partial (a'(u))^2}{\partial r_i} = 2\left[(N_i'(u)r''(u) + r'(u)N_i''(u)) - a'(u)\frac{\partial a}{\partial r_i}\right]$$

$$\frac{\partial (a'(u))^2}{\partial z_i} = 2\left[(N_i'(u)z''(u) + z'(u)N_i''(u)) - a'(u)\frac{\partial a}{\partial z_i}\right]$$

$$\frac{\partial H(u)}{\partial r_i} = \frac{1}{(a(u))^3}\frac{\partial b(u)}{\partial r_i} - \left[\frac{3b(u)}{(a(u))^4} + \frac{z(u)'}{r(u)(a(u))^2}\right]\frac{\partial a(u)}{\partial r_i} - \frac{z'(u)N_i(u)}{(r(u))^2 a(u)}$$

$$\frac{\partial H(u)}{\partial z_i} = \frac{1}{(a(u))^3}\frac{\partial b(u)}{\partial z_i} - \left[\frac{3b(u)}{(a(u))^4} + \frac{z(u)'}{r(u)(a(u))^2}\right]\frac{\partial a(u)}{\partial z_i} + \frac{N_i'(u)}{r(u)a(u)}$$

With the last calculations, the derivatives of the curvature energy, the volume, the area and A can easily be worked out.
Using (eq.2.1), (eq.3.2) and (eq.3.3) to transform the integral, the derivatives of the curvature energy, can be written as

$$\frac{\partial E_{HC}}{\partial r_i} = 2\pi\int_{u=0}^{u=1}\frac{\kappa}{2}\left[2(H(u) - C_0)a(u)r(u)\frac{\partial H(u)}{\partial r_i} + (H(u) - C_0)^2\left(r(u)\frac{\partial a(u)}{\partial r_i} + a(u)N_i(u)\right)\right]du$$

$$\frac{\partial E_{HC}}{\partial z_i} = 2\pi \int_{u=0}^{u=1} \frac{\kappa}{2} \left[2(H(u) - C_0)a(u)r(u)\frac{\partial H(u)}{\partial z_i} + (H(u) - C_0)^2 r(u)\frac{\partial a(u)}{\partial z_i} \right] du$$

and the numerical integration can be computed with (eq.3.4).

The same process is applied to the derivatives of the volume, of the area and of A:

$$\frac{\partial S}{\partial r_i} = 2\pi \int_{u=0}^{u=1} \left[r(u)\frac{\partial a(u)}{\partial r_i} + a(u)N_i(u) \right] du \qquad \frac{\partial S}{\partial z_i} = 2\pi \int_{u=0}^{u=1} r(u)\frac{\partial a(u)}{\partial z_i} du$$

$$\frac{\partial V}{\partial r_i} = 2\pi \int_{u=0}^{u=1} z'(u)r(u)N_i(u)du \qquad \frac{\partial V}{\partial z_i} = 2\pi \int_{u=0}^{u=1} \frac{(r(u))^2}{2} N_i'(u)du$$

$$\frac{\partial A}{\partial r_i} = 2\pi \int_{u=0}^{u=1} \left[(a'(u))^2 \left(r(u)\frac{\partial a(u)}{\partial r_i} + N_i(u)a(u) \right) + \frac{\partial (a'(u))^2}{\partial r_i} a(u)r(u) \right] du$$

$$\frac{\partial A}{\partial z_i} = 2\pi \int_{u=0}^{u=1} \left[(a'(u))^2 r(u)\frac{\partial a(u)}{\partial z_i} + \frac{\partial (a'(u))^2}{\partial z_i} a(u)r(u) \right] du$$

Finally, F and its gradient can be evaluated.

4.2.2 Choice of the parameters

The choice of the constants of penalization k_1, k_2 and k_3 is important.

First, they do not play the same role: the conservation of the volume and of the aera

is more important than the conservation of the velocity of the parametrization $a(u)$. So, the ratios between the parameters are significant.

Moreover, it is not recommanded to use high values because the system will be too rigid.

Atfer some tests, the set of parameters to get an equilibrium position of minimum energy and with the surface and the volume prescribed is

$$k_1 = 10 \qquad k_2 = 10 \qquad k_3 = 10^{-4}$$

4.2.3 Matlab function

Matlab offers a lot of functions which facilate the resolutions of the problems. The function FMINCON finds a minimum of a constrained nonlinear multivariable function under some constraints. In this study, they are linear equalities. One have to write them in matrix formulation to use the Matlab function:

$$\begin{bmatrix} 1 & 0 & 0 & 0 & ... & 0 & 0 & 0 & 0 \\ 0 & 1 & 0 & -1 & ... & 0 & 0 & 0 & 0 \\ 0 & 0 & 0 & 0 & 1 & 0 & 0 & 0 & 0 \\ 0 & 0 & 0 & 0 & ... & -1 & 0 & 1 & 0 \\ 0 & 0 & 0 & 0 & ... & 0 & 0 & 0 & 1 \end{bmatrix} \begin{bmatrix} \boldsymbol{P} \end{bmatrix} = \begin{bmatrix} 0 \\ 0 \\ z_0(\text{middle point}) \\ 0 \\ 0 \end{bmatrix}$$

This system holds for the boundary conditions for the closed vesicles. If the vesicles are open, the system is reduced at the 2 first rows.

The variables defining the shape of the curve are the control points. Therefore the minimization will search within the position of these points.

The parameters of the function FMINCON are chosen in order to find the equilibrium with enough precision.

In the following table we compare the volume and the area prescribed and obtained for four cases (Fig.4.3 and Fig.4.4)

type of shape	area prescribed	area obtained	volume presribed	volume obtained
oblate	314.1593	314.1331	471.2389	471.2504
discocyte	314.1593	314.1377	314.1593	314.1730
prolate	314.1593	314.1379	471.2389	471.2483
dumbbell	314.1593	314.1364	408.4070	408.4186

Table 4.1: Comparison between the volume and area prescribed and obtained.

4.3 Phase diagrams

4.3.1 Types of axisymmetric shape

We are going to study two different branches of axisymmetric shape: the prolate - dumbbell - pear-shaped vesicle (which are related to budding), the oblate - discocyte - stomatocyte (Fig.4.2).

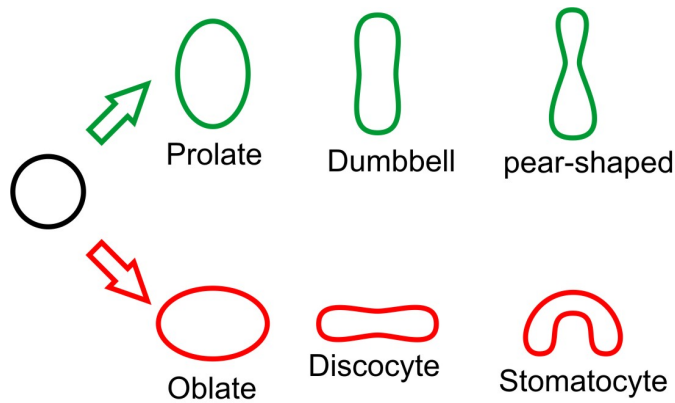

Figure 4.2: Different vesicle shapes.

In the spontaneous curvature model, most of the transitions between the different types of shape are discontinuous while they are continuous for the bilayer-coupling model, another representation of the lipid bilayer. This fact will introduce difficulties in the numerical study of transitions.

The prolate-dumbbell and the oblate-discocyte shapes are easier to obtain than the stomatocyte and the pear-shapes vesicle because the transitions are continuous.

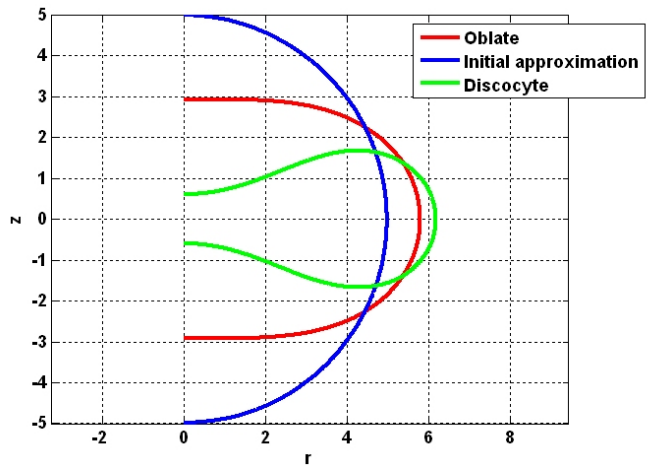

Figure 4.3: Shape of minimum of energy for a volume, an area and a spontaneous curvature : oblate and discocyte.

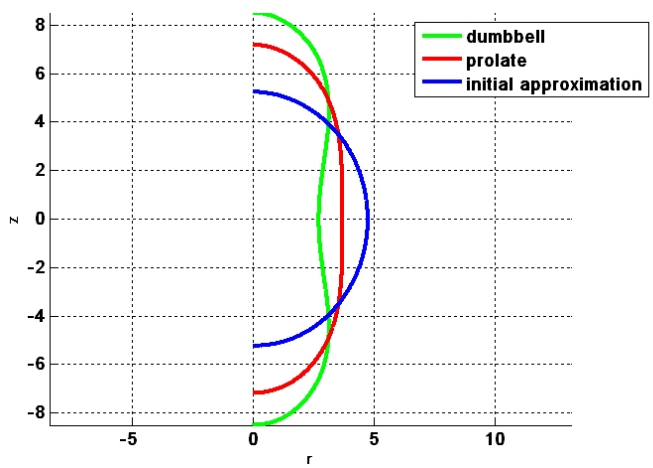

Figure 4.4: Shape of minimum of energy for a volume, an area and a spontaneous curvature given: prolate and dumbbell.

Two different parameters have a strong influence over the shape obtained: the ratio volume-area of the vesicle and the spontaneous curvature C_0. Their values define

the type of shape the vesicle will take.

As the bending energy is scale invariant, the phase diagram and the energy diagram are constructed thanks to three dimensionless parameters[2], which are the reduced volume

$$v = \frac{V(\mathbf{P})}{\frac{4\pi}{3}R_0^3}$$

the reduced spontaneous curvature

$$c_0 = C_0 R_0$$

and a ratio of the energy

$$\frac{E_{HC}}{8\pi\kappa}.$$

To obtain different equilibrium positions and make paths in the phase diagram, the next method is applied.

[2]Two for each graph.

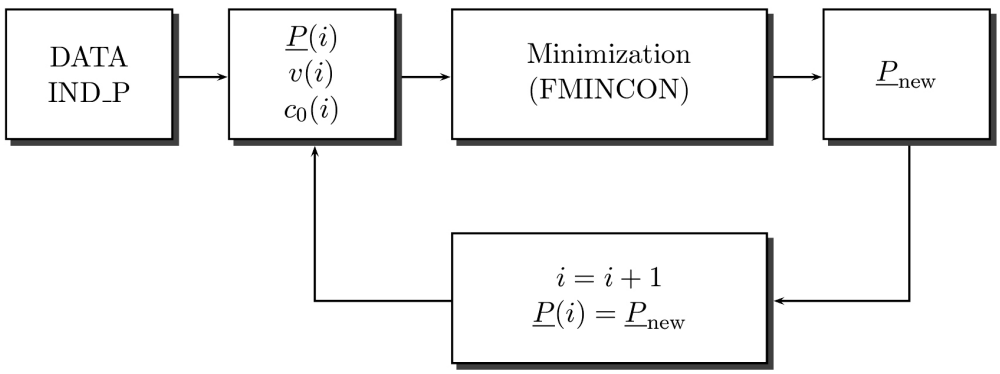

Figure 4.5: Diagram of the program for the static study.

DATA and INDP are Matlab structures array which contain respectively all the data of the problem and all the parameters independent of the position of the breakpoints.

A path of different values of the reduced volume and of the spontaneous curvature is applied. To implement this, we define two vectors which contain all the values of the reduced volume and of the spontaneous curvature the system will take:

$$v = [1\ 0.95\ 0.9\ 0.85\ 0.8\ 0.75\ 0.7] \qquad \text{and} \qquad c_0 = [0\ 0.2\ 0.4\ 0.6\ 0.8\ 1\ 1.2].$$

Then, first we search the equilibrium for $v(1)$ and $c_0(1)$ with the matlab optimization function. Starting from this state, the second position of equilibrium (corresponding to the next set of parameters): $v(2)$ and $c_0(1)$) is calculated. The same is applied until the end of the vector v. After, the reduced volume is set to $v(end)$ and the spontaneous curvature changed from $c_0(1)$ to $c_0(end)$. Only one parameter is changed at every step.

In this way, some consecutive positions of equilibrium are obtained.

We will consider first the simplest case of a spontaneous curvature equal to zero. This case will give a good display of the behaviour of the system.

4.3.2 Case 1: Spontaneous curvature equal to zero

In this case, the vesicle can evolve in two different ways. The first starts with the prolates and finishes with the dumbbells. As we can see in the following graph (Fig.4.6), the pear-shaped vesicles do not exist in this case. The second begins with the oblates and ends with the discocytes/stomatocytes (Fig.4.2).

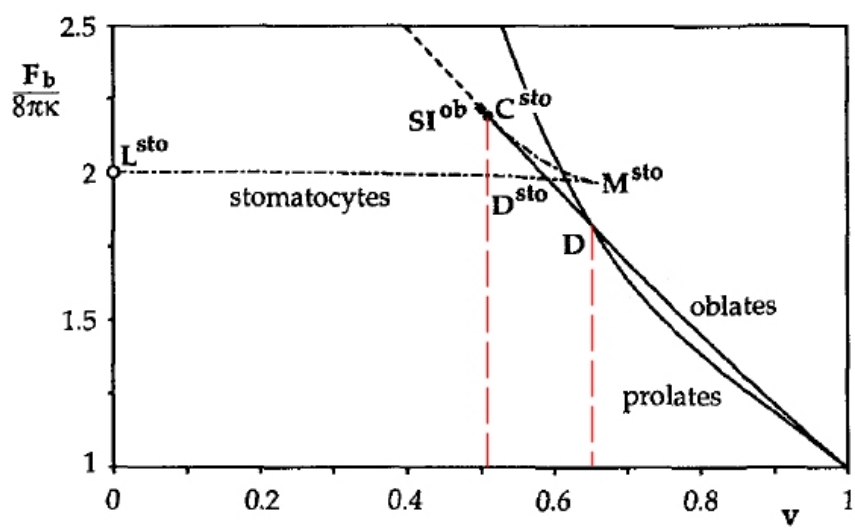

Figure 4.6: Bending energy in function of the reduced volume and the type of shape for the spontaneous curvature model and for $C_0 = 0$ [8].

As first approximation, we take a slight disformed sphere to display the oblate-discocyte case ($r_{def} = 1.01r$, $z_{def} = 0.99z$) and the opposite for the prolate-dumbbell case ($r_{def} = 0.99r$, $z_{def} = 1.01z$).
The discontinuity between the stomatocyte and the discocyte is too great and it is not possible to compute it with a curvature energy equal to zero.

The first analyzed case is the transformation from an oblate to a discocyte.
In the graphs below (Fig.4.7 and Fig.4.8), the shape evolution and the corresponding energy are displayed. The figure 4.7 shows the curve in the $r - z$ plane. One can point out that the evolution of energy matches the one of figure 4.6: the line named "oblate". The evolution is linear and, as the reduced volume decreases, the energy increases because the shape has more curvature.

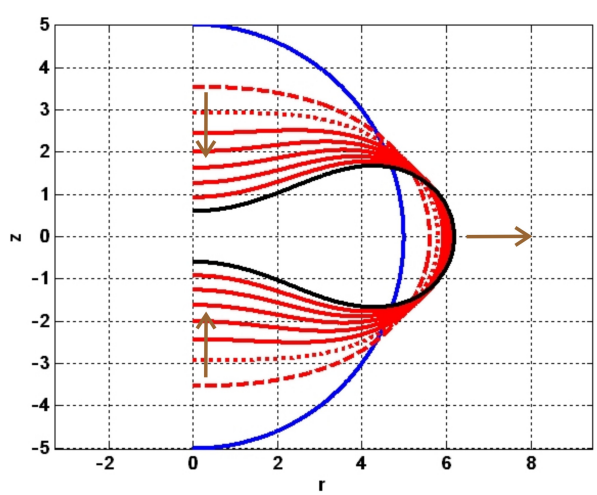

Figure 4.7: Evolution from an oblate to a discocyte by decrease of the reduced volume from 1 until 0.6.

At the end, the reduced volume is 0.6, the energy corresponding is 1.95. It is the same as in the phase diagram (Fig. 4.6).

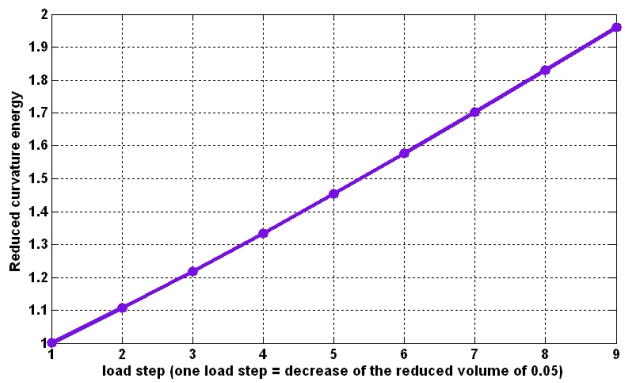

Figure 4.8: Variation of the energy in function of the reduced volume for the transformation oblate-discocyte.

Then, the transition from a prolate to a dumbbell is displayed. The reduced volume decreases from 1 until 0.6 and the energy reaches 2.2.
The principal difference is the variation of the energy which is not linear anymore. Because of this competition between the linear and the non-linear energy curve, at the beginning the shape of minimum energy is the prolate and when the reduced volume reaches $v = 0.65$, the shape of minimum energy becomes the oblate (Fig. 4.6).

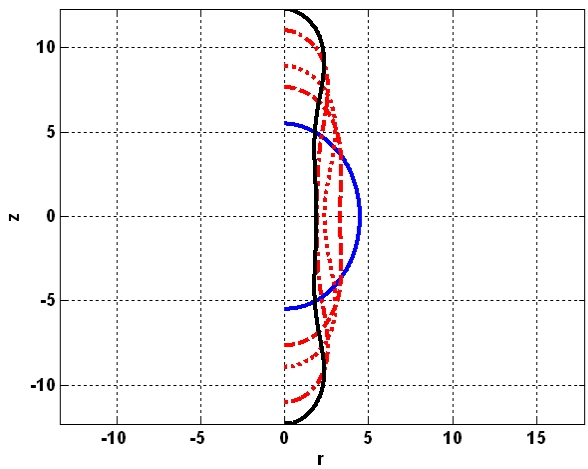

Figure 4.9: Evolution from an prolate to a dumbbell by decrease of the reduced volume.

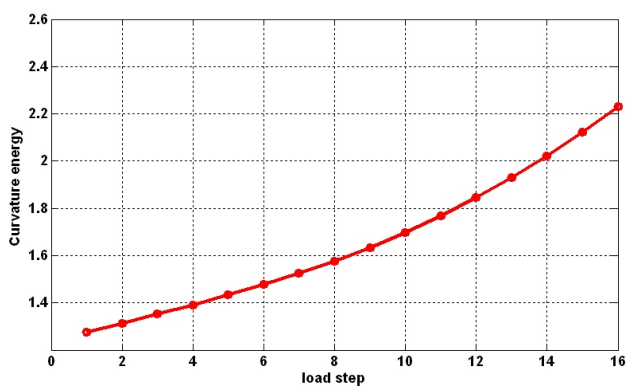

Figure 4.10: Variation of the energy in function of the reduced volume for the transformation prolate-dumbbell.

4.3.3 Case 2: Spontaneous curvature different from zero

By changing the two parameters (volume and spontaneous curvature), more shapes are displayed. We will compare our results with the phase diagram for the spontaneous

curvature (Fig.4.11) [8]

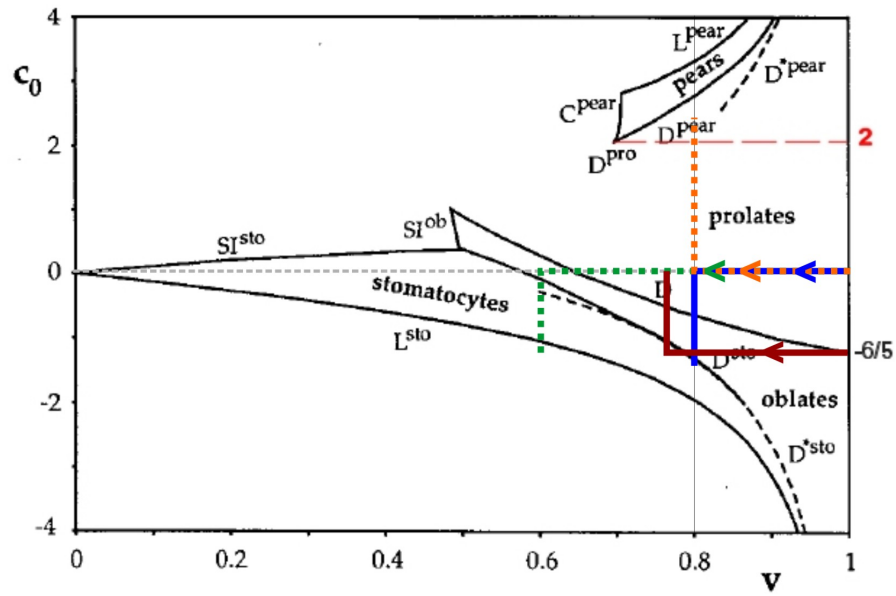

Figure 4.11: Phase diagram for the spontaneous curvature model.

Some of the transitions are discontinuous and are represented in this graph with a line whose name starts with a D. There exist places in the diagram that have not been explained yet[3].

First, the stomatocytes are computed. Different sorts of stomatocytes are showed depending on the reduced volume. The first method is to start with a sphere of nil spontaneous curvature as initial aproximation and to decrease the volume slowly. Then the spontaneous curvature is changed in order to obtain stomatocyte. For the stomatocyte, the spontaneous curvature has to be positive[4].

[3]Under the L_{sto} line and after the SI lines.

[4]This is the contrary of the diagram (Fig.4.6) but it is just a question of definition of the curve parametrization.

The first test is to reduce the volume until $v = 0.8$ and then change the spontaneous curvature until $c_0 = 1.3$. The stomatocyte is obtained in the last change: $v = 0.8$ and $c_0 = 1.3$. In the following graph (Fig. 4.12 and Fig.4.13), the gap is clear between the discocyte and the stomatocyte states. The geometric change between the discocyte and the stomatocyte is discontinuous.

At first, the energy is more or less constant (for the two first iteration), this is related to the change of reduced volume. When the spontaneous curvature begins to change, the energy increases a lot. And then, when the stomatocyte is obtained, the increase of energy vanishes (after the blue line)(Fig.4.14).

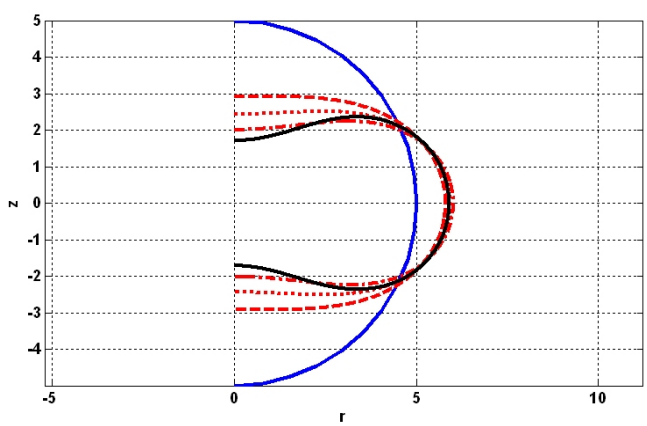

Figure 4.12: Evolution from an oblate to a discocyte by variation of the reduced volume and of the spontaneous curvature. At the end, for the curve in black, the parameters are $v = 0.8$ and $c_0 = 1.2$.

This fact can be explained by the examination of the curvature of the different shapes. For a spontaneous curvature equal to zero and a volume and area equal to

the one of the sphere, the shape of minimum energy is the sphere. When the volume decreases, the shape has to modify itself and the discocyte is displayed. However, this leads to an raise of the energy because the mean curvature increases. When a spontaneous curvature different from zero is enforced, the energy growths too. Then, while the changes of shape are discontinuous, the discocyte changes instantaneously into a stomatocyte. This allows a decrease of the energy because the part of spontaneous curvature added is compensated by the one of the shape (which is not symmetric anymore with the plane $r = 0$).

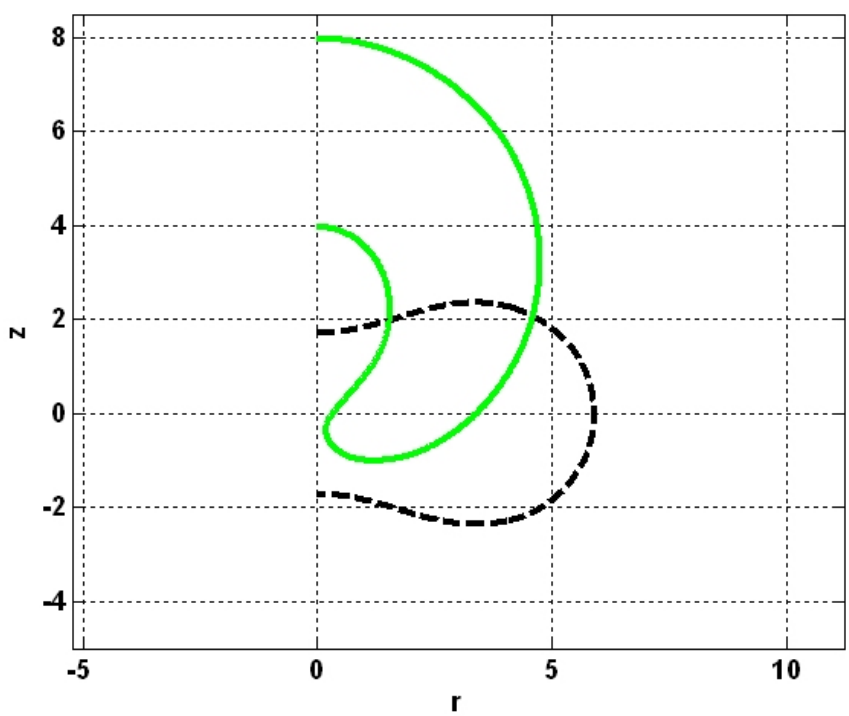

Figure 4.13: Discontinuous transformation from a discocyte ($v = 0.8$ and $c_0 = 1.2$) into a stomatocyte ($v = 0.8$ and $c_0 = 1.3$).

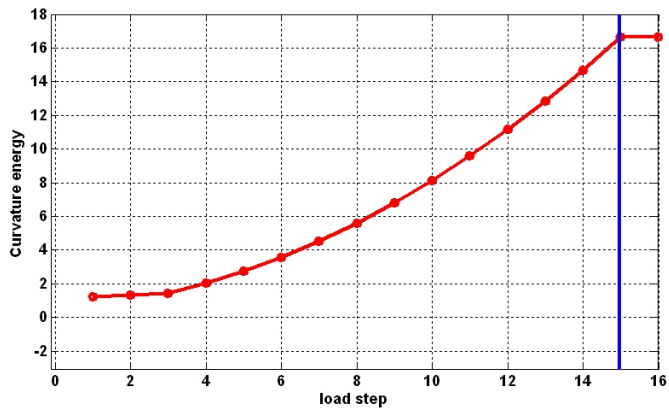

Figure 4.14: Variation of the energy in function of the reduced volume for the transformation oblate-stomatocyte.

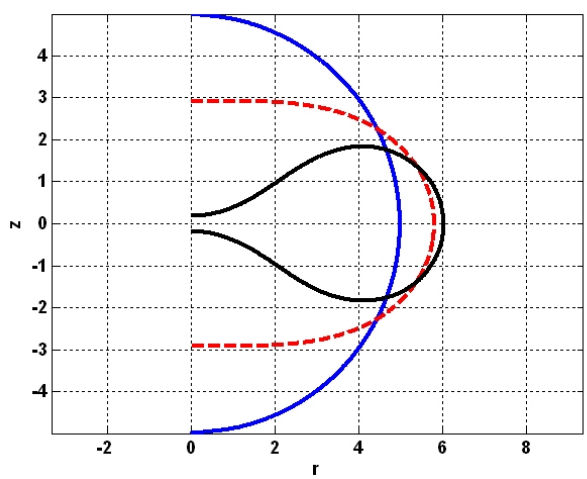

Figure 4.15: Evolution from an oblate to a discocyte by variation of the reduced volume and the spontaneous curvature.

The second test is the same as the first but the reduced volume is decreased until $v = 0.6$ in place of $v = 0.8$. The stomatocyte obtained is a bit different: the formation of an intern sphere can be seen. In the figure 4.15, the first and the last

position respectively correspond to a set of parameters of

$$v = 1 \quad \text{and} \quad c_0 = 0, \qquad v = 0.6 \quad \text{and} \quad c_0 = 0.6.$$

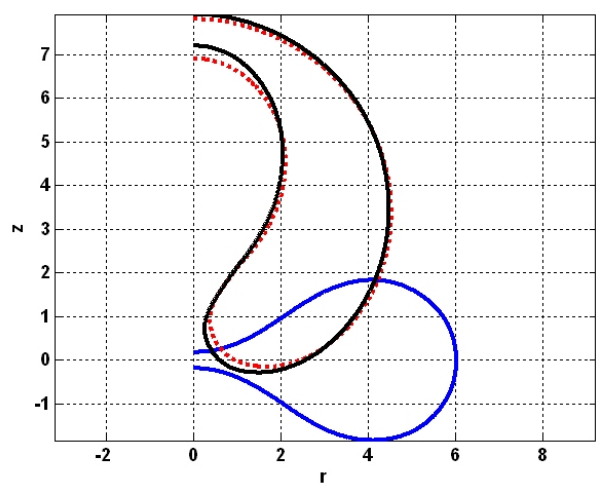

Figure 4.16: Discontinuous transformation from a discocyte to stomatocytes.

The figure 4.16 shows the discontinuous transformation from a discocyte ($v = 0.6$ and $c_0 = 0.6$) into a first stomatocyte ($v = 0.6$ and $c_0 = 0.7$) in red dot line and another ($v = 0.6$ and $c_0 = 1.3$) in black.

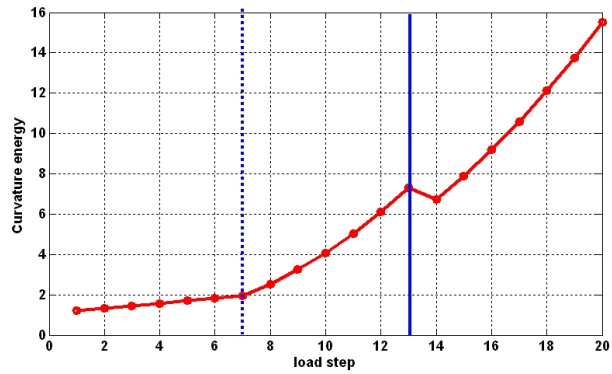

Figure 4.17: Variation of the energy in function of the reduced volume for the transformation oblate-stomatocyte.

The energy increases when the curvature of the shape increases. While the discocyte changes into a stomatocyte, the energy decreases. In fact, as the spontaneous curvature is different from zero, the vesicle tends to have more curvature in one way (positive for the stomatocyte). To minimize its curvature energy with a spontaneous curvature different from zero, the vesicle displays a shape non-symmetric with the plane $r = 0$: the stomatocyte. This is logical considering the definition of the curvature energy (eq. 2.1).

Now, a different branch of the diagram is studied: the prolates. While the volume decreases, the energy increases sensibily. As the spontaneous curvature is added (after the dot-line in Fig. 4.20), the energy decreases, stabilizes and then increases one more time. At the blue line, there is a discontinuous transition between the dumbbell and the pear-shaped vesicle. This type of transformation is related to budding. The type of finite elements implemented does not allow the separation of the curve in two different curves. So, the two different vesicle are linked with a small neck. This leads

to a shape of the type of a tube (Fig.4.18 ,Fig.4.19 and Fig.4.20).

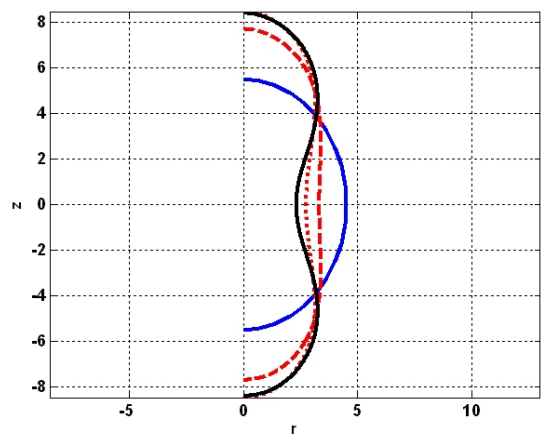

Figure 4.18: Evolution from a prolate to a dumbbell by variation of the reduced volume and the spontaneous curvature. At the end, for the curve in black, the parameters are $v = 0.8$ and $c_0 = 0$.

In this case, the spontaneous curvature added to display the pear-shaped vesicle is negative (the opposite to the one that leads to the stomatocyte shape).
The pear-shaped vesicle can be explained in the same way as the stomatocyte. As one enforces a spontaneous curvature different from zero, the system reacts to decrease the energy corresponding. This is possible with a shape which is no longer symmetric with the plane $r = 0$: the pear-shaped vesicle .

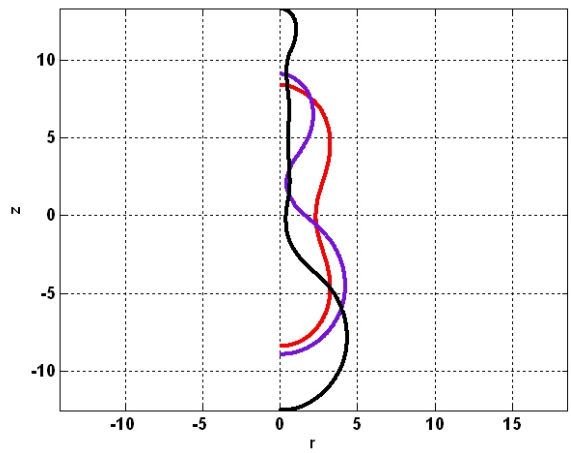

Figure 4.19: Discontinuous transformation from a dumbbell (in red, $v = 0.8$ and $c_0 = 0$) into a pear-shaped vesicle (in mallow, $v = 0.8$ and $c_0 = -1.2$) and then in a tube (in black, $v = 0.8$ and $c_0 = -2.2$) .

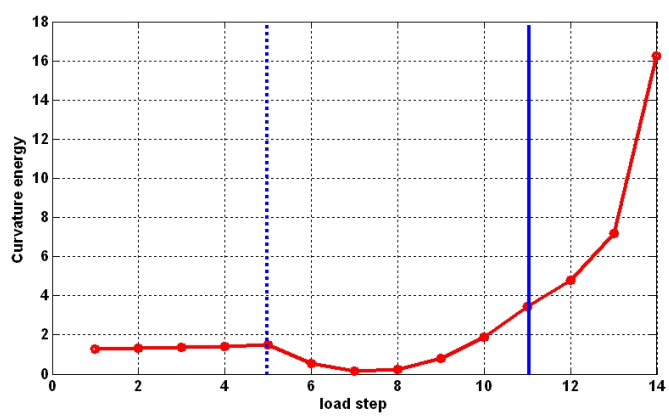

Figure 4.20: Variation of the energy in function of the reduced volume for the transformation prolate-tube

The last test is different. The spontaneous curvature is different from zero at the beginning. Then, the reduced volume is decreased to obtain a stomatocyte. At the

end, the spontaneous curvature is changed until zero and the discocyte is displayed one more time.

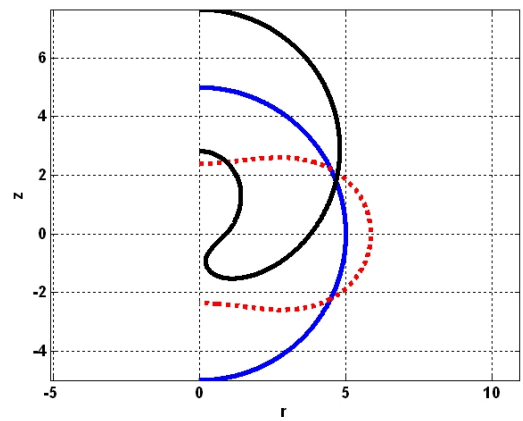

Figure 4.21: Evolution from an discocyte (in red dot line) to a stomatocyte (in black) by variation of the reduced volume and the spontaneous curvature.

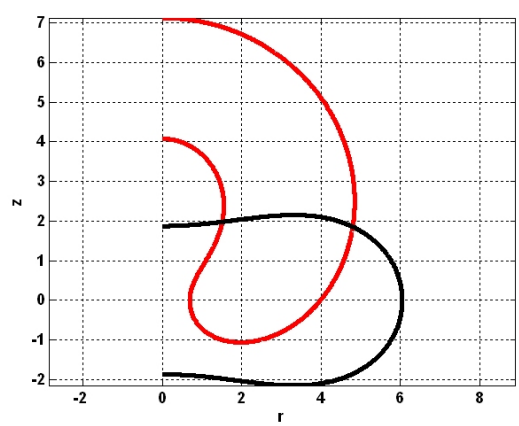

Figure 4.22: Evolution from an stomatocyte (in red) to a discocyte(in black) by variation of the reduced volume and the spontaneous curvature.

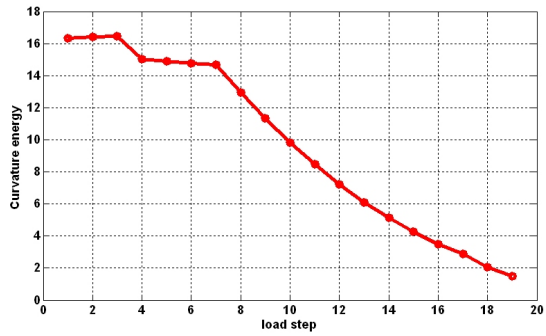

Figure 4.23: Variation of the energy in function of the reduced volume for the transformation discocyte-stomatocyte-discocyte.

The first shape is a discocyte in red dot line in the figure 4.21 for $v = 0.88$ and $c_0 = 1.2$, then the discocyte transforms into a stomatocyte for $v = 0.84$ and $c_0 = 1.2$. The next graph (Fig. 4.22) displays the inverse transformation: the stomatocyte ($v = 0.78$ and $c_0 = 0.2$) changes into a discocyte ($v = 0.78$ and $c_0 = 0$).
The energy only decreases for this path. Actually at the beginning, the spontaneous curvature is different from zero, therefore, a decrease of the reduced volume decrease the energy until a certain point. Then, the spontaneous curvature is changed until zero, and the energy follows decreasing.

Chapter 5

Dynamic study

5.1 Introduction

The dynamics of the problem are governed by the dissipation and by the curvature energy. Two kinds of dissipation will be studied. The first one is the dissipation related to the Willmore flow or L_2 dissipation and the second one is the inner flow dissipation which models the dissipation of energy as the lipids move on the bilayer to accommodate shape changes. The evolution in time of the shape and the energy corresponding is displayed for both methods.

Some interesting dynamic cases are studied with an explicit scheme in time.

5.2 Mechanical analogy

The dynamics of the vesicle can be compared with a mechanical system formed by a spring and a dashpot in parallel (Fig.5.1). The dashpot represents the mechanics which dissipate the energy in time, it is function of the velocity of the system. The spring is the device which stores potential energy and absorbes the energy propor-

tionally to the velocity.

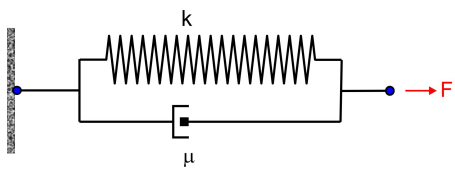

Figure 5.1: Mechanical analogy: dashpot and spring in parallel

Equations governing the mechanical system:

$$E_k = \frac{1}{2}k(x - l_0)^2$$

$$W_D = \frac{1}{2}\mu\dot{x}^2$$

One can define the energy release rate as the energy dissipated by unit of time

$$G_k = -\dot{E}_k$$

The dynamics of the system can be found as the minimum of the difference between the energy release rate G_k and the dissipation energy W_D

$$min(W_D - G_k) = 0. \tag{5.1}$$

This system could lead to different equilibrium positions in function of the dissipation used (Fig.5.2). However, in our case, the time evolution is so small that the equilibrium found will be the same.

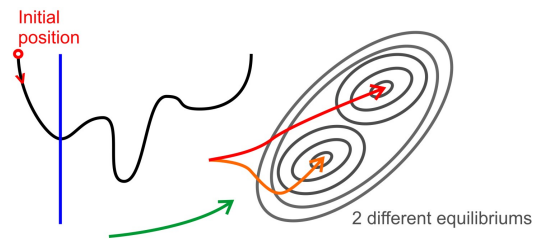

Figure 5.2: Different equilibriums.

The same can be done with the dynamics of the vesicle. The energy will be the curvature energy and the dissipation can be either the L_2 dissipation or the innerflow dissipation.

To find the evolution of the surface of the vesicle in time, the first step is to calculate the field of velocity on the surface (Fig. 5.3). Then, the position of the control points at time $n + 1$ will be found using a a forward Euler method.

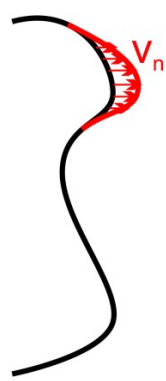

Figure 5.3: Field of normal velocities on the curve at time n.

As we use an explicit scheme, the value of the time step has to be small enough.

5.3 Mathematical process

5.3.1 Setup and discretization

We consider an axisymmetric representation of surfaces through the generating curve. This curve is represented parametrically using B-Splines approximants (chapter 3). We discretize other quantities defined on the surface in a similar way, for instance the normal velocity and the tangential velocity (here both are scalar quantities)

$$v_n(u) = \sum_{i=1}^{N+1} v_{ni} N_i(u), \quad v_t(u) = \sum_{i=1}^{N+1} v_{ti} N_i(u).$$

The pressure or surface tension, when needed, has to be interpolated with lower-order approximants, e.g. first-order B-Splines (linear finite elements)

$$p(u) = \sum_{i=1}^{N+1} p_i \hat{N}_i(u).$$

A tangent unit vector to the surface in the u direction and a unit normal are (Fig.5.4)

$$\boldsymbol{t} = \frac{1}{a}\{r', z'\}, \qquad \boldsymbol{n} = \frac{1}{a}\{-z', r'\}$$

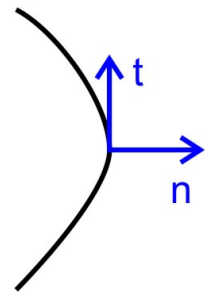

Figure 5.4: Tangential and normal vector on the curve.

The velocity of the surface is

$$\boldsymbol{v} = \{\dot{r}, \dot{z}\},$$

hence

$$v_t = \frac{1}{a}(r'\dot{r} + z'\dot{z}), \qquad v_n = \frac{1}{a}(-z'\dot{r} + r'\dot{z})$$

5.3.2 Governing equations

One needs to collect all the dissipation potentials into the functional $W[v_t, v_n]$, here quadratic in the velocities. The energetic mechanisms depend essentially on the shape of the surface, and are collected in $\Pi[\boldsymbol{x}]$. We can compute their rate of change $\dot{\Pi}[v_t, v_n]$, which depends parametrically on the shape (in the same way that W does) and is linear on the velocities. We typically have (linear) local constraints on the velocities, which we write as $c(v_t, v_n) = 0$. We can also have global shape constraints $C[\boldsymbol{x}] = 0$, which we linearize into $\dot{C}[v_t, v_n] = 0$. The dynamics equilibrate the dissipative and the energetic forces, or minimize $W + \dot{\Pi}$ with respect to v_t and v_n subject to the constraints (section 5.2). Forming the Lagrangian

$$\mathcal{L}[v_t, v_n, \lambda](\Lambda) = W[v_t, v_n] + \dot{\Pi}[v_t, v_n] - \int_\Gamma \lambda c(v_t, v_n)\, dS - \Lambda \dot{C}[v_t, v_n]$$

we find the velocities at each configuration given by $\boldsymbol{x}$ by finding stationary points, i.e.

$$\delta_{v_t}\mathcal{L} = \delta_{v_n}\mathcal{L} = \delta_\lambda\mathcal{L} = \delta_\Lambda\mathcal{L} = 0$$

for all possible variations. In a Galerkin finite element method, we allow for variations of the form $\delta v_t = \delta v_n = N_I$, $\delta\lambda = \hat{N}_I$. Naturally, we identify λ with the surface tension or 2D pressure.

The update of the surface is then performed explicitly from

$$\dot{r} = \frac{1}{a}(r'v_t - z'v_n), \qquad \dot{z} = \frac{1}{a}(z'v_t + r'v_n),$$

i.e.

$$r^{n+1} = r + \frac{\Delta t}{a}(r'v_t - z'v_n), \qquad z^{n+1} = z + \frac{\Delta t}{a}(z'v_t + r'v_n),$$

where unless the superscript $^{n+1}$ is present, everything is evaluated at $t = t^n$. Since the B-Splines shape functions are not interpolatory, it makes more sense to perform this update using a least-squares approach, i.e. minimizing

$$\int_\Gamma \left(\frac{r^{n+1} - r}{\Delta t} - \frac{1}{a}(r'v_t - z'v_n)\right)^2 dS$$

which leads to the linear systems

$$\sum_J \int_\Gamma N_I N_J \, dS \; r_J^{n+1} = \int_\Gamma \left[r + \frac{\Delta t}{a}(r'v_t - z'v_n)\right] N_I \, dS \tag{5.2}$$

$$\sum_J \int_\Gamma N_I N_J \, dS \; z_J^{n+1} = \int_\Gamma \left[z + \frac{\Delta t}{a}(z'v_t + r'v_n)\right] N_I \, dS \tag{5.3}$$

subject to the constraints

$$r_1^{n+1} = 0, \quad r_n^{n+1} = 0, \quad z_1^{n+1} = z_2^{n+1}, \quad z_n^{n+1} = z_{n-1}^{n+1}.$$

5.3.3 Energetic contributions

Curvature elasticity

As seen before (2.1), we consider the curvature energy

$$E_{HC} = \int_\Gamma \frac{\kappa}{2}(H - C_0)^2 \, dS.$$

Its energy release rate is [1]

$$\begin{aligned} G_{HC} = -\dot{E}_{HC} \quad &= \quad -\int_\Gamma \frac{\kappa}{2}(H - C_0)\left[2\Delta v_n + (H^2 - 4K + HC_0)v_n\right] \, dS \\ &\quad -\kappa\pi r(H - C_0)^2(\pm 1)v_t\big|_{boundary} \end{aligned}$$

The plus/minus sign comes from the sign of $\partial/\partial u \cdot \boldsymbol{\nu}$. (ν) is the exterior normal at the end of the surface (Fig. 5.5).

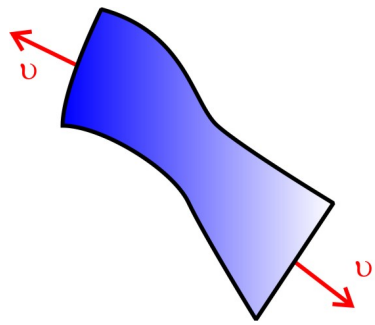

Figure 5.5: Normal exterior of the surface.

For axisymmetric surfaces, we have

$$\Delta v_n = \frac{1}{ar}\frac{\partial}{\partial u}\left(\frac{r}{a}\frac{\partial v_n}{\partial u}\right) = \frac{1}{ar}\left[\frac{r'a - ra'}{a^2}v_n' + \frac{r}{a}v_n''\right].$$

Consequently, the nodal forces can be computed as follows:

$$f_I^{HC,v_n} = \delta G_{HC}\cdot N_I = -\int_\Gamma \frac{\kappa}{2}(H - C_0)\left\{2\frac{1}{ar}\left[\frac{r'a - ra'}{a^2}N_I' \right. \right. \tag{5.4}$$

$$\left. \left. + \frac{r}{a}N_I''\right] + (H^2 - 4K + HC_0)N_I\right\} 2\pi ar\ du \tag{5.5}$$

$$f_1^{HC,v_t} = \kappa\pi r(H - C_0)^2\big|_{u=0}, \qquad f_n^{HC,v_t} = -\kappa\pi r(H - C_0)^2\big|_{u=1}$$

5.3.4 Dissipative contributions

L_2 dissipation

The L_2 dissipation is (eq.2.2)

$$W_{L_2}[v_n] = \frac{\hat{\mu}}{2}\int_\Gamma v_n^2 dS.$$

Its variation follows as

$$\delta W_{L_2} = \hat{\mu}\int_\Gamma v_n \delta v_n \; dS$$

which results in the stiffness terms

$$K_{IJ}^{L_2,v_n,v_n} = \hat{\mu}\int_\Gamma N_I N_J 2\pi a r du$$

Inner flow dissipation

The physical inner flow dissipation reads (eq.2.3)

$$W_D[v_t, v_n] = \mu\int_\Gamma \left\{ \left(\frac{1}{a}v_t'\right)^2 + \left(\frac{r'}{ar}v_t\right)^2 - \frac{2v_n}{a}\left(\frac{b}{a^3}v_t' + \frac{z'r'}{ar^2}v_t\right) + (H^2 - 2K)v_n^2 \right\} dS$$

Its variation is

$$\begin{aligned} \delta W_D &= 2\mu\int_\Gamma \left\{ \frac{1}{a^2}v_t'\delta v_t' + \left(\frac{r'}{ar}\right)^2 v_t\delta v_t - \frac{v_n}{a}\left(\frac{b}{a^3}\delta v_t' + \frac{z'r'}{ar^2}\delta v_t\right)\right\} dS + \quad (5.6)\\ &\quad 2\mu\int_\Gamma \left\{ -\frac{1}{a}\left(\frac{b}{a^3}v_t' + \frac{z'r'}{ar^2}v_t\right) + (H^2 - 2K)v_n \right\}\delta v_n dS \quad (5.7)\end{aligned}$$

which results in the stiffness contributions

$$K_{IJ}^{D,v_t,v_t} = 2\mu \int_\Gamma \left\{ \frac{1}{a^2} N_I' N_J' + \left(\frac{r'}{ar} \right)^2 N_I N_J \right\} 2\pi a r \; du$$

$$K_{IJ}^{D,v_n,v_n} = 2\mu \int_\Gamma (H^2 - 2K) N_I N_J 2\pi a r \; du$$

$$K_{IJ}^{D,v_n,v_t} = -2\mu \int_\Gamma \frac{1}{a} N_I \left(\frac{b}{a^3} N_J' + \frac{z'r'}{ar^2} N_J \right) 2\pi a r \; du, \qquad K_{IJ}^{D,v_t,v_n} = K_{JI}^{D,v_n,v_t}$$

5.3.5 Constraints

Volume constraint

Assuming the surface has no free end, this single constraint is simply

$$Cst = \dot{V} = -\int_\Gamma v_n (2\pi a r) \; du$$

where the constant can be either nil or different from zero depending on the case studied.

The resulting constraint vector is

$$L_I^{vol,v_n} = -\int_\Gamma N_I 2\pi a r \; du$$

Global area constraint

This single constraint is simply

$$0 = \dot{S} = -\int_\Gamma H v_n \; dS \pm 2\pi r v_t \big|_{boundary}.$$

The resulting constraint vector is

$$L_I^{area,v_n} = -\int_\Gamma H N_I 2\pi a r \; du$$

and if free boundaries are present, one of the following terms may be present

$$L_1^{area,v_t} = -2\pi r(0), \qquad L_n^{area,v_t} = 2\pi r(1)$$

Local area constraints

The weak statement of the constraint is

$$0 = -\int_\Gamma p[\frac{(rv_t)'}{ar} - Hv_n]dS$$

which results in the constraint matrices

$$L_{IJ}^{p,v_t} = -\int_\Gamma \hat{N}_I \left(r' N_J + r N_J'\right) 2\pi du, \qquad L_{IJ}^{p,v_n} = \int_\Gamma \hat{N}_I H N_J 2\pi a r du$$

5.3.6 Boundary conditions

For a symmetry boundary point, one has for each configuration that $r = 0$ and $z' = 0$. The time-evolution needs to preserve these conditions, hence

$$\dot{r} = \dot{z}' = 0, \quad \text{at symmetry end-points.}$$

Recalling the identities

$$\dot{r} = \frac{1}{a}(r' v_t - z' v_n), \qquad \dot{z} = \frac{1}{a}(z' v_t + r' v_n)$$

we obtain the constraints

$$r'(u)v_{ti} - z'(u)v_{ni} = 0, \quad \text{with } u = 0, i = 1 \text{ and/or } u = 1, i = n$$

which reduce to $v_{t1} = 0$ and/or $v_{tn} = 0$, and also, at $u = 0$ for simplicity (an analogous expression is obtained at $u = 1$), we have

$$\left(z'' - \frac{z'a'}{a}\right)_{u=0} v_{t1} + \left(r'' - \frac{r'a'}{a}\right)_{u=0} v_{n1} + z'(0)\sum_{i=1}^{3} N_i'(0)v_{ti} + r'(0)\sum_{i=1}^{3} N_i'(0)v_{ni} = 0.$$

This constraint simplifies to

$$\left(r'' - \frac{r'a'}{a}\right)_{u=0} v_{n1} + r'(0)\sum_{i=1}^{3} N_i'(0)v_{ni} = 0.$$

The constraint matrices are then (to be modified if one end is free)

$$\boldsymbol{L}^{BCs,v_t} = \begin{bmatrix} 1 & 0 & \dots & 0 \\ 0 & \dots & 0 & 1 \end{bmatrix}$$

$$L_{1J}^{BCs,v_n} = \begin{bmatrix} \left(r'' - \frac{r'a'}{a}\right)_{u=0} + r'(0)N_1'(0) & r'(0)N_2'(0) & r'(0)N_3'(0) & 0 & \dots & 0 \end{bmatrix}$$

$$L_{2J}^{BCs,v_n} = \begin{bmatrix} 0 & \dots & 0 & r'(1)N_{n-2}'(1) & r'(1)N_{n-1}'(1) & r'(1)N_n'(1) + \left(r'' - \frac{r'a'}{a}\right)_{u=1} \end{bmatrix}$$

5.3.7 L_2 gradient flow with exact global area and volume constraints

Now, we consider $\boldsymbol{K}^{L_2,v_n,v_n}$, $\boldsymbol{K}^{L_2,v_t,v_t}$, $\boldsymbol{f}^{HC}$, and the constraints given by $\boldsymbol{L}^{BCs}$, $\boldsymbol{L}^{vol}$ and $\boldsymbol{L}^{area}$

and the system to solve is

$$\begin{bmatrix} \boldsymbol{K}_{tot} & \boldsymbol{L_{tot}} \\ \boldsymbol{L_{tot}}' & \boldsymbol{0} \end{bmatrix} \begin{bmatrix} \boldsymbol{v} \\ LM \end{bmatrix} = \begin{bmatrix} \boldsymbol{f}^{HC} \\ \boldsymbol{f}^{LM} \end{bmatrix}$$

with

$$\boldsymbol{K}_{tot} = \begin{bmatrix} \boldsymbol{K}^{L_2,v_n,v_n} & \boldsymbol{0} \\ \boldsymbol{0} & \boldsymbol{K}^{L_2,v_t,v_t} \end{bmatrix}$$

and

$$\boldsymbol{L}_{tot} = \begin{bmatrix} \boldsymbol{L}^{BC} & \boldsymbol{L}^{vol} & \boldsymbol{L}^{area} \end{bmatrix}$$

where $\boldsymbol{L}^{BC}$ depends on the case of boundary used and LM the Lagrangian multiplicators and $\boldsymbol{f}^{LM}$ the rigth-hand side corresponding to the Lagrangian conditions.

5.3.8 Inner flow dissipation with exact local area and volume constraint

In this case, we consider $\boldsymbol{K}^{D}$, $\boldsymbol{f}^{HC}$, $\boldsymbol{L}^{BCs}$, $\boldsymbol{L}^{p}$ and $\boldsymbol{L}^{vol}$

and the system to solve is

$$\begin{bmatrix} \boldsymbol{K}_{tot} & \boldsymbol{L_{tot}} \\ \boldsymbol{L_{tot}}' & \boldsymbol{0} \end{bmatrix} \begin{bmatrix} \boldsymbol{v} \\ LM \end{bmatrix} = \begin{bmatrix} \boldsymbol{f}^{HC} \\ \boldsymbol{f}^{LM} \end{bmatrix}$$

with

$$\boldsymbol{K}_{tot} = \begin{bmatrix} \boldsymbol{K}^{D,v_n,v_n} & \boldsymbol{K}^{D,v_n,v_t} \\ \boldsymbol{K}^{D,v_t,v_n} & \boldsymbol{K}^{L_2,v_t,v_t} \end{bmatrix}$$

and

$$\boldsymbol{L}_{tot} = \left[\begin{array}{ccc} \boldsymbol{L}^{BC} & \boldsymbol{L}^{vol} & \boldsymbol{L}^{p} \end{array} \right]$$

where $\boldsymbol{L}^{BC}$ depends on the case of boundary used and LM the Lagrangian multiplicators and $\boldsymbol{f}^{LM}$ the rigth-hand side corresponding to the Lagrangian conditions.

This case of dissipation is a local definition and so, the translations (rigid body motions) do not dissipate energy. To avoid these cases of moves, one has to fix a point and so there is one more boundary consition.

5.4 Program

To implement the dynamics of the vesicle, the following steps are followed (Fig.5.6). The first state is one of equilibrium calculated before in the static part. Then, one (or two) of its parameters is changed brutally (spontaneous curvature for example). To reach the new equilibrium, the system has to move. Two sorts of dissipations are used and the evolutions in time are different.

The velocities (normal and tangential) at the control points are found and help to update the curve. The interpolation of these velocities at the Gauss points of the curve are done in order to calculate the position of the breakpoints in time $n + 1$ thanks to (eq. 5.2) and (eq.5.3).

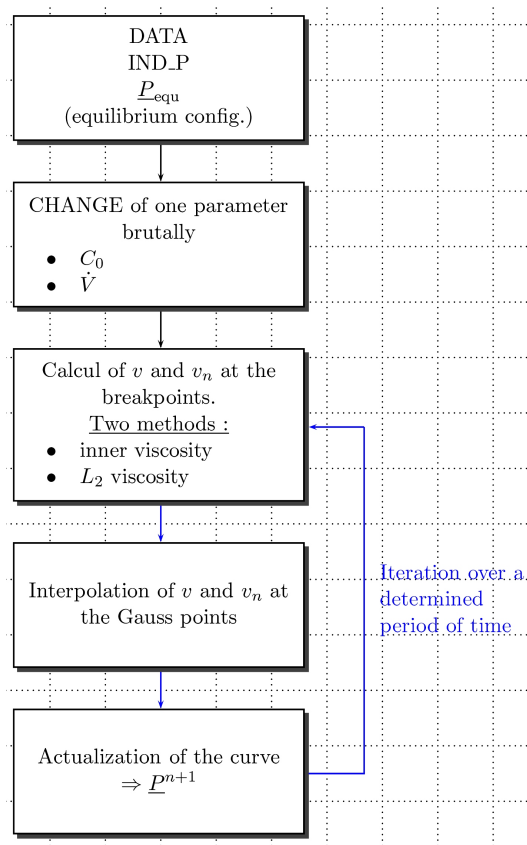

Figure 5.6: Diagram of the dynamic program.

5.5 Reparametrization

The deformations are great and so, sometimes the breakpoints cannot move as much as they want on the curve and stay all in the same part.

This is bad and prevents us from finding the good evolution of the vesicle in time.

To resolve this problem a reparametrization is done everytime the system reaches a certain time or when there is too much difference between the shortest and the longest distance between two breakpoints.

We use a minimization function of Matlab (FMINUNC) to calculate the reparametrization but it is not so efficient because we do not give it the gradient of the function we want to minimize.

5.6 Dynamic evolution

With the program implemented, the dynamics can be study in a lot of ways. However, as the program takes a very long time to give the results, only a few cases are analysed.

First, one has to choose the initial position. The choice is made to take an equilibrium position with a spontaneous curvature different from zero and a reduced volume different from one.

Then , there is two methods to put our shape out of its equilibrium: the first is to change suddenly the spontaneous curvature. It can be enforced to be zero or the one of the sphere. The second is to enforce the variation of volume ($\dot{V}$) to be different from zero until reaching the volume of the sphere.

The dynamics are calculated for the both cases: inner and $L2$ viscosities.

The numerical parameters are taken equal for the both to make a good comparison of the dynamics.

Choice of parameters

The parameters of the program are the following.

First, there are the parameters of the model : μ_{inner}, μ_t and μ_v. They are taken equal

to 1.

Second, one has to choose the parameter of the time-scheme: Δt. It is taken equal to 0.00002 for the stomatocyte transformation and equal to 0.000125 for the pear-shaped one.

Third, the parameters of the reparametrization are chosen. The constant of reparametrization is taken equal to $1e5$. If we use a lower value, sometimes, the reparametrization fails because it is not rigid enough. We choose to reparametrize every 101 step-time for the stomatocyte and every 201 step-time for the prolate because it evolves less accumulation of control points during the transformation.

Finally, for the pear-shaped - prolate transformation, the only change to put the system out-of equilibrium is the change of the spontaneous curvature. It is posed equal to zero. In the case of the stomatocyte, the spontaneous curvature is posed equal to the one of the sphere ($C_0 = \frac{-2}{R_{sphere}}$) and the volume is changed until it reaches the one of the sphere.

5.6.1 Pear-shaped vesicle - prolate

The study of the transformation of a pear-shaped vesicle into a dummbbell is done using the both viscosities.

Dynamics

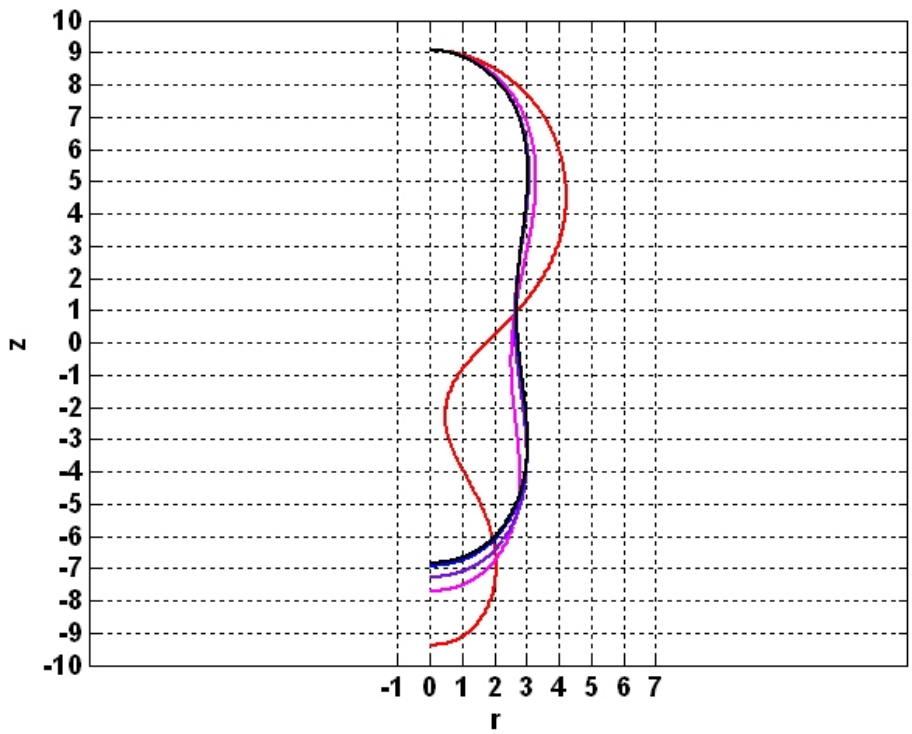

Figure 5.7: Dynamics of the transformation pear-shaped vesicle - dumbbell with the inner-flow viscosity.

One can see that the evolution in time is different for the different viscosities.
In figure 5.7, the inner-flow viscosity is used. The results for $L2$ viscosity is displayed at figure 5.8. For both graphics, the first state is represented in red and the last state in black. Between them, the evolution follows the pink , mallow and then blue line.

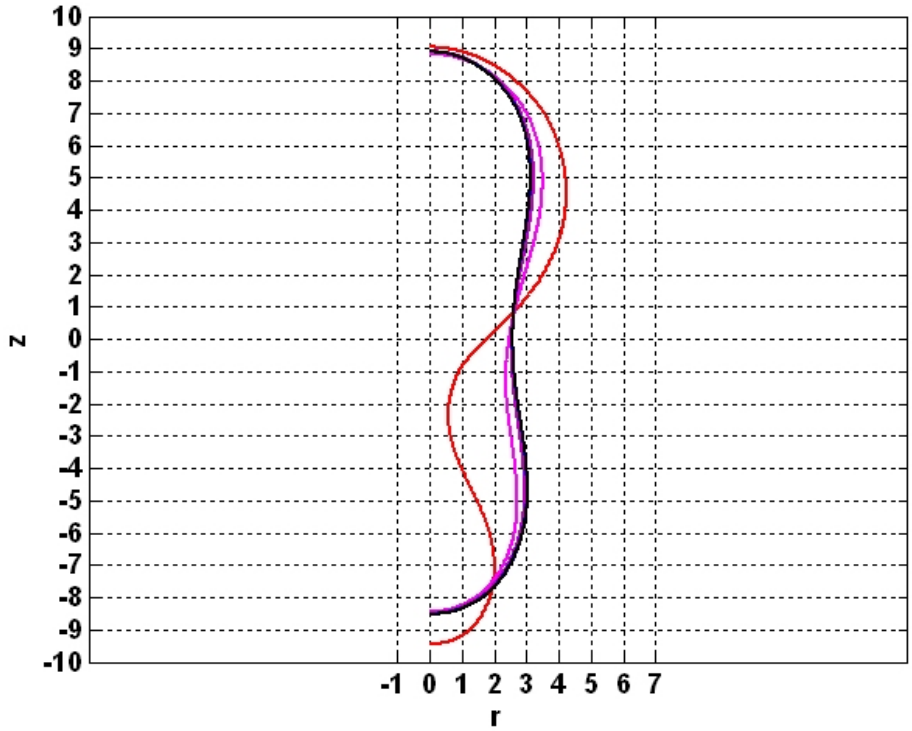

Figure 5.8: Dynamics of the transformation pear-shaped vesicle - dumbbell with the $L2$ viscosity.

The evolution for the inner-flow viscosity shows that the pear-shaped vesicle transforms itself into a dumbbell passing by states where the little "head" of the pear stay more longer small. Just at the end, the two parts become equal.
Differently, the evolution for the $L2$ viscosity shows that the two head of the pear tend to nearly egalize themselve at the beginning.
Furthermore, the final equilibriums are different in fonction of the viscosity used: the one of the inner-flow is shorter (in the z direction), the other shorter in the r direction.

5.6.2 Stomatocyte - discocyte

In this case, only a part of the transformation process is showed because there are numerical problems (with the reparametrization).

Dynamics

In this example, the differences of the evolutions can clearly be analyzed.
In the inner-flow case (Fig.5.10), the stomatocyte tends to put out the sphere it contains. The right part of the vesicle do not move.

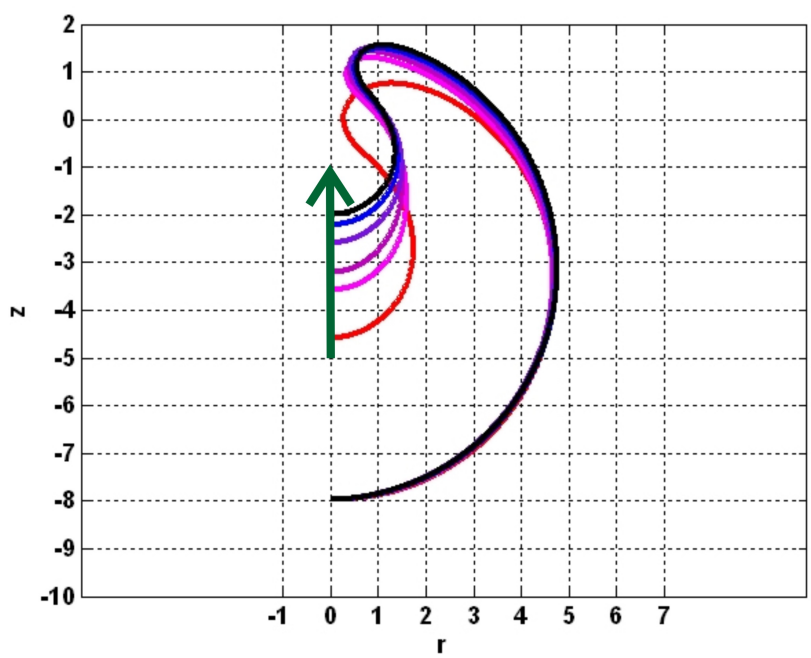

Figure 5.9: Dynamics of the transformation stomatocyte - discocyte with the inner-flow viscosity.

The graphics of the $L2$ viscosity shows that the stomatocyte tends to open out to get a discocyte.

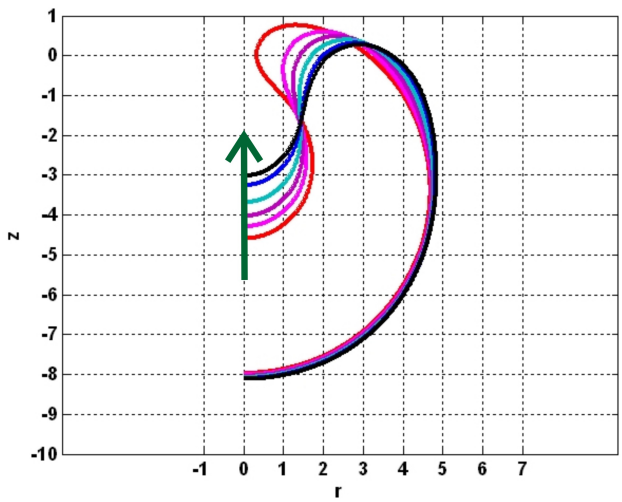

Figure 5.10: Dynamics of the transformation stomatocyte - discocyte with the $L2$ viscosity.

Energy evolution

There are problems in the dynamics for the inner-flow dissipation as we can see in the curve of energy (Fig5.11).

In fact, every time a breakpoint has to pass the higher point of the curve, it leads to a pic of energy. To avoid this, one solution is to implement a better reparametrization or to use a model with more breakpoints.

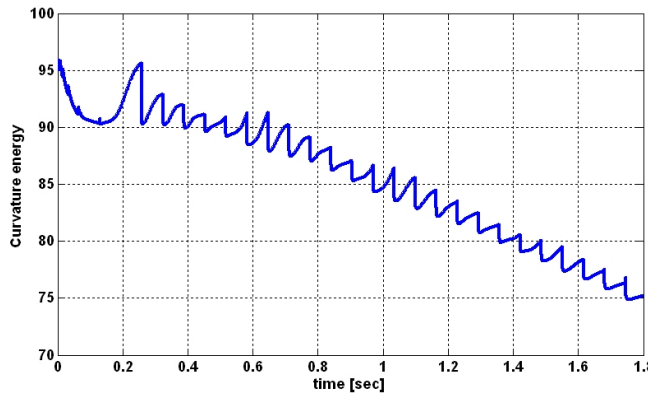

Figure 5.11: Evolution of the energy in time for the stomatocyte transformation with the inner-flow dissipation.

The evolution of energy for the $L2$ viscosity is displayed at figure 5.12. There are small instabilities in the beginning of the transformation. It could come from the reparametrization.

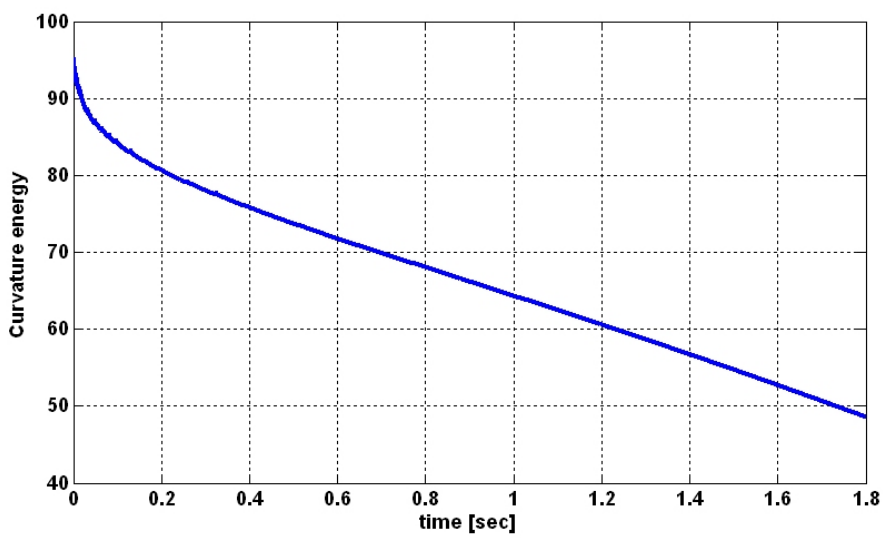

Figure 5.12: Evolution of the energy in time for the stomatocyte transformation with $L2$ dissipation.

$3D$ representation

The $3D$ representation of the last case is displayed below. It allows to imagine better the shape and the intern sphere.

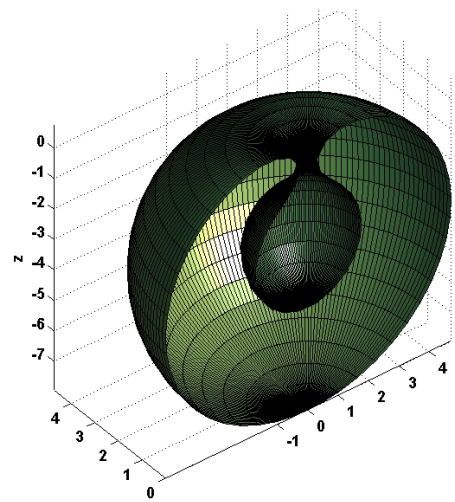

Figure 5.13: Initial stomatocyte- cross section.

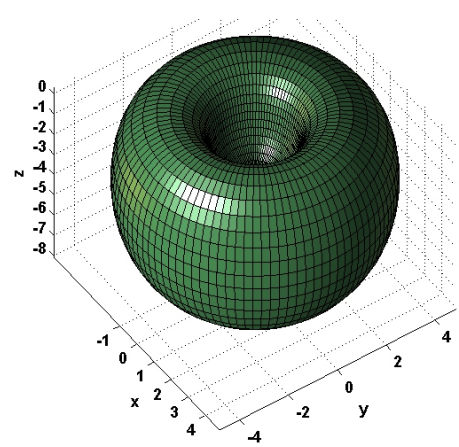

Figure 5.14: Final stomatocyte with the $L2$ viscosity.

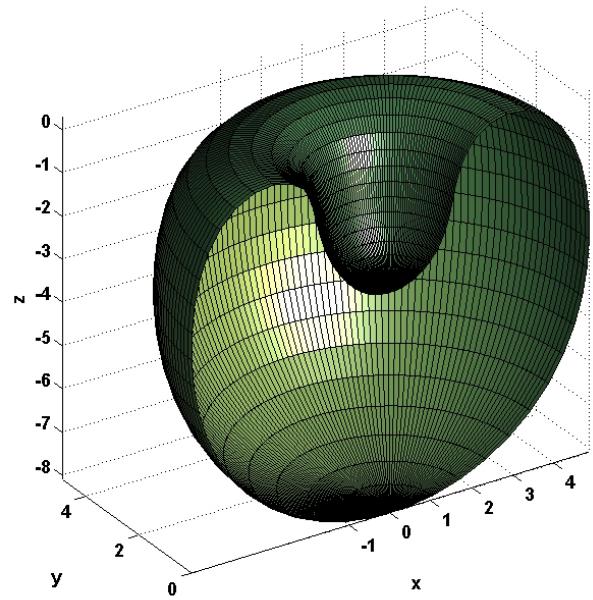

Figure 5.15: Final stomatocyte with the $L2$ viscosity - cross section.

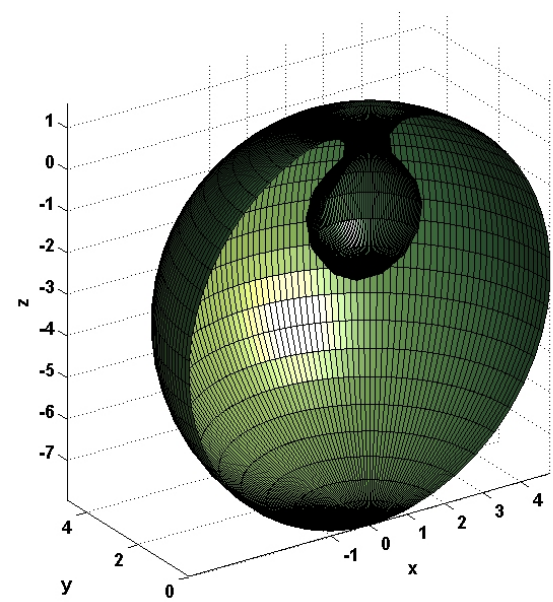

Figure 5.16: Final stomatocyte with the inner-flow viscosity - cross section.

Chapter 6

Conclusion

This project models the dynamics of fluid membranes, with an emphasis on the effect of the inner flow dissipation. This is the lateral motion within the membrane surface of the fluid particles making up the membrane.
The first two chapters recall some biologic aspects of the problem, the hypothesis taken and explain the numerical modelization and implementation chosen.
In the static part, the equilibrium shapes and the paramaters related are found: prolate, pear-shaped vesicle, tube, oblate, discocyte and stomatocyte. Paths in the phase diagram for the spontaneous curvature are modelized and our results are compared to it.
Then, the dynamic study is done, using two different dissipations and the evolution in time are clearly different. It shows that the dissipation, often neglected by the scientists is important and worth to be well modelized to clearly represent the physics of the problem.

This work is the beginning of a larger study. Actually, some method used are very simple and not enough accurate and can easily be improved.
In the dynamic part, we used an explicit temporal scheme which slows down the

program because the time-step needed to have a stable scheme is very small for this model. One first improvement would be to implement an implicit time-scheme for the dynamic part.

Moreover, the reparametrization used is not very efficient. This leads to a lot of annoying problems during the tests. A new method is necessary to improve the program and to get more accurate results.

Other ideas of study could be to use another representation of the asymmetry of the bilayer: the area-difference model. It is more complex to implement but all the shape-transitions are continuous and therefore it is easier to display the change of shapes numerically.

On the other hand, this project only modelizes vesicles of one component. The line tension between two different components which induced budding can be modelized to have a more realistic model [11]. To represent the entire budding, the last thing to add, is the separation of one vesicle in two. This kind of study was done before [12] and leads to a lot of different and interesting shapes but this study is not realistic biologically speaking.

These are some ideas which would allow us to go deeper into in the subject but there are many more ways of study: non-asymmetric shapes, topologicaly variant shapes, others energetic mechanisms (outer flow, flip-flop, ...), interactions [13].

One can see that this subject is very large and that our study is just a little part of it. Much more work is needed to modelize the biology accurately.

Bibliography

[1] M. Arroyo and A. DeSimone. Continuum modeling and simulation of the dynamics of fluid membranes. *In preparation*, 2008.

[2] Jim Thomas. Cell parts. http://en.wikibooks.org/wiki/Image:Cell_parts.png.

[3] Mariana Ruiz. Cell membrane detailed diagram. http://en.wikipedia.org/wiki/Image:Cell_membrane_detailed_diagram.svg, 2007.

[4] Daniel Balas and Patrick Philip. Cours d'histologie générale. Universite de Nice Sophia Antipolis, Faculté de Médecine - GRTV, Service d'Histologie, 2001-2002. http://homepage.mac.com/danielbalas/HISTOLOGIE/HISTGENE/histgen1/histgen5/histgen5.htm.

[5] Stephen L. Kimzey, Craig L. Fischer, Philip C. Johnson, Stephan E. Ritzmann, and Charles E. Mengel. *Biomedical Results of Apollo*, chapter Hematology and immunology studies. BioTechnology.

[6] Joshua Nosanchuk and Arturo Casadevall. Scanning electron micrograph of a budding cell of cryptococcus neoformans in the presence of l−dopa (the parental cell is approx. 5μ m in diameter). http://mic.sgmjournals.org/content/vol149/issue8/cover.shtml.

[7] Jane Wang. Inex pharmaceuticals corporation. http://www.bioteach.ubc.ca/Bio-industry/Inex.

[8] U. Seifert and R. Lipowsky. *Handbook of Biological Physics*, volume 1, chapter Morphology of Vesicles. Elsevier Science B.V., 1995.

[9] L.E. Scriven. Dynamics of a fluid interface: equations of motion for newtonian surface fluids. *Chem. Eng. Sci.*, 12:98–108, 1960.

[10] Les A. Piegl and Wayne Tiller. *The NURBS book*. Springer Verlag, 1997.

[11] F. Jülicher and R. Lipowsky. Shape transformations of vesicles with intermembrane domains. *Physical Review E*, 53(3):2670–2683, 1996.

[12] Q. Du, C. Liu, R. Ryham, and X. Wang. Modeling vesicle deformations in flow fields via energetic variational approaches. *Nonlinearity*, submitted, 2005.

[13] R. Lipowsky. The morphology of lipid membranes. *Current Opinion in Structural Biology*, 6:531–540, 1995.